

Jet-vetoed Higgs cross section in gluon fusion at $N^3LO+NNLL$ with small- R resummation

Andrea Banfi,¹ Fabrizio Caola,² Frédéric A. Dreyer,^{2,3,4} Pier F. Monni,⁵ Gavin P. Salam,^{2,*} Giulia Zanderighi,^{2,5} Falko Dulat⁶

¹*Department of Physics and Astronomy, University of Sussex, Brighton BN1 9RH, UK*

²*CERN, PH-TH, CH-1211 Geneva 23, Switzerland*

³*Sorbonne Universités, UPMC Univ Paris 06, UMR 7589, LPTHE, F-75005, Paris, France*

⁴*CNRS, UMR 7589, LPTHE, F-75005, Paris, France*

⁵*Rudolf Peierls Centre for Theoretical Physics, University of Oxford, Oxford OX1 3NP, UK*

⁶*Institute for Theoretical Physics, ETH Zürich, 8093 Zürich, Switzerland*

ABSTRACT: We present new results for the jet-veto efficiency and zero-jet cross section in Higgs production through gluon fusion. We incorporate the N^3LO corrections to the total cross section, the NNLO corrections to the 1-jet rate, NNLL resummation for the jet p_t and LL resummation for the jet radius dependence. Our results include known finite-mass corrections and are obtained using the jet-veto efficiency method, updated relative to earlier work to take into account what has been learnt from the new precision calculations that we include. For 13 TeV collisions and using our default choice for the renormalisation and factorisation scales, $\mu_0 = m_H/2$, the matched prediction for the jet-veto efficiency increases the pure N^3LO prediction by about 2% and the two have comparable uncertainties. Relative to NNLO+NNLL results, the new prediction is 2% smaller and the uncertainty reduces from more than 10% to less than 5%. Results are also presented for the central scale $\mu_0 = m_H$.

* On leave from CNRS, UMR 7589, LPTHE, F-75005, Paris, France

Contents

1	Introduction	1
2	Outline of the formalism	3
2.1	Updated jet-veto efficiency method at fixed order	3
2.2	Resummation	5
2.3	Matching	6
2.4	Jet-radius dependence and small- R effects	8
2.5	Quark-mass corrections	10
3	$N^3LO+NNLL+LL_R$ cross section and 0-jet efficiency at 13 TeV	12
4	Conclusions	15
A	Revisited JVE uncertainty prescription	17
B	Choice of the central scale	23
C	Small-R correction factor	26

1 Introduction

Since the announcement of the discovery of the Higgs boson [1, 2], a dynamic research programme has come into place to measure and constrain its properties. The precision of the measurements is already such that the interpretation of data is sometimes limited by theoretical uncertainties (see e.g. Refs. [3, 4]). Experimental errors will decrease in Run II, because of the higher luminosity and of the higher energy. Experimental analyses will also benefit from the experience gained in Run I, which will result in optimised Higgs analyses already from the early stages of Run II.

The dominant Higgs-production mode at the LHC is gluon-gluon fusion. The most fundamental quantity is the total Higgs production cross-section, which allows one to compute the total number of Higgs bosons produced at the LHC for a given energy and luminosity. In some Higgs boson decay modes (most notably WW^* and $\tau\tau$), it is standard to perform different analyses depending on the number of accompanying jets. This is because different jet multiplicities have different dominant backgrounds. Of particular importance for the WW decay is the zero-jet case, where the dominant top-quark decay background is dramatically reduced. For precision studies it is important to predict accurately the fraction of signal events that survive the zero-jet constraint, and to assess the associated theory uncertainty. Jet-veto transverse momentum thresholds used by ATLAS and CMS are relatively soft ($\sim 25 - 30$ GeV), hence QCD real radiation is severely constrained by the cut

and the imbalance between virtual and real corrections results in logarithms of the form $\ln(p_{t,\text{veto}}/m_H)$ that should be resummed to all orders in the coupling constant. This resummation has been carried out to next-to-next-to-leading logarithmic accuracy (NNLL, i.e. including all terms $\alpha_s^n \ln^k(p_{t,\text{veto}}/m_H)$ with $k \geq n - 1$ in the logarithm of the cross section) and matched to next-to-next-to-leading order (NNLO) in Refs. [5–7] (some of the calculations also included partial N³LL contributions). At this order one finds that the effect of the resummation is to shift central predictions only moderately, and to reduce somewhat the theoretical uncertainties. Yet, the residual theoretical uncertainty remains sizeable, roughly 10% [5], and the impact of higher-order effects could therefore be significant.

Since the first NNLO+NNLL predictions for the jet-veto, three important theoretical advances happened: firstly, the N³LO calculation of the total gluon-fusion cross section [8]; secondly the calculation of the NNLO corrections to the Higgs plus one-jet cross-section [9–11]; and finally the LL resummation of logarithms of the jet-radius R [12]. Given these recent advances, we are now in a position to improve on the previous prediction by extending the matching of the jet-veto cross-section to N³LO+NNLL+LL_{*R*}. In order to perform the matching and to estimate the uncertainties one needs to extend the matching schemes introduced in Ref. [5] to one order higher. In doing so, we will also revisit the formulation of the “jet-veto efficiency” (JVE) approach that was introduced in Ref. [13].

For accurate predictions it is also important to investigate the impact of finite quark masses, a subject extensively discussed in the literature. Finite quark-mass effects are known exactly only up to NLO [14–19]. The impact of top quark effects on the leading jet’s transverse momentum at NLO has been studied through a $1/m_t$ expansion [20]. Different prescriptions have been proposed to include top and bottom effects in analytic resummations [21–23] as well as parton-shower simulations, e.g. in (N)NLO+PS generators [24–26]. Here, we include exact mass effects up to NNLL+NLO and study the impact of the resummation scale associated with the bottom and top-bottom-interference contributions. Mass effects at NNLO and N³LO are currently unknown, so we use the large- m_t limit (without any rescaling) at these orders.

This paper is organised as follows. In Sec. 2.1 we recall the Jet Veto Efficiency (JVE) method, and we give a new prescription for the uncertainty estimate. This differs from the one given in ref. [5], and we believe is more appropriate now that the Higgs total production and Higgs plus one-jet cross sections are known respectively through N³LO and NNLO. In the rest of Sec. 2, we introduce the various ingredients of the calculation, and we discuss how they are combined together. In Sec. 3 we present our new results at 13 TeV centre-of-mass energy, while Sec. 4 contains our conclusions. In Appendix A we further motivate the introduction of the new JVE uncertainty prescription. In Appendix B we compare our final predictions obtained with central scale $m_H/2$ to predictions obtained with central scale m_H . Finally, in Appendix C we give some technical details about the small- R resummation.

2 Outline of the formalism

2.1 Updated jet-veto efficiency method at fixed order

The core element of our estimate of uncertainty in the jet-vetoed cross section is the JVE method [23]. The premise of the method is that the zero-jet cross section is given by the product of the total cross section and jet-veto efficiency and that the uncertainties in the two quantities are largely uncorrelated. The argument that motivates this working assumption is that, at small p_t , uncertainties in the efficiency are due to non-cancellation of real and virtual contributions, while those in the total cross section are connected with the large K -factor that is observed in going from leading order to higher orders.

The JVE method can be applied both at fixed order and with resummation.¹ It is useful to first extract the jet-veto efficiency from the total Higgs cross section σ_{tot} and the cross section $\Sigma(p_{t,\text{veto}})$ for Higgs production with a jet veto (i.e. without any jets with $p_t > p_{t,\text{veto}}$). We define the expansion of the total cross section and of the jet-veto cross-section up to perturbative order $\mathcal{O}(\alpha_s^{2+n})$ as

$$\sigma_{\text{tot},n} = \sum_{i=0}^n \sigma^{(i)}, \quad \Sigma(p_{t,\text{veto}}) = \sigma^{(0)} + \sum_{i=1}^n \Sigma^{(i)}(p_{t,\text{veto}}). \quad (2.1)$$

Furthermore we use $\bar{\Sigma}(p_{t,\text{veto}})$ to denote (minus) the cross section to have at least one jet above a scale $p_{t,\text{veto}}$. Its order α_s^{2+i} component is given by

$$\bar{\Sigma}^{(i)}(p_{t,\text{veto}}) = - \int_{p_{t,\text{veto}}}^{\infty} dp_t \frac{d\Sigma^{(i)}(p_t)}{dp_t}. \quad (2.2)$$

This is related to $\Sigma^{(i)}(p_{t,\text{veto}})$ via

$$\Sigma^{(i)}(p_{t,\text{veto}}) = \sigma^{(i)} + \bar{\Sigma}^{(i)}(p_{t,\text{veto}}). \quad (2.3)$$

From the above equations it is evident that one can obtain $\Sigma^{(i)}(p_{t,\text{veto}})$ at a given order in α_s by combining the inclusive cross-section and the $H + 1$ jet cross-section, both computed at the same order in α_s . Recently the $i = 3$ coefficient was computed both for σ_{tot} [8] and for $\bar{\Sigma}^{(i)}(p_{t,\text{veto}})$ [9–11].

The most obvious definition for the jet-veto efficiency $\epsilon(p_{t,\text{veto}})$ is to write it as a ratio $\Sigma(p_{t,\text{veto}})/\sigma_{\text{tot}}$ using the highest order available in each case. We call this prescription “(a)” and at N³LO it reads

$$\epsilon^{(a)}(p_{t,\text{veto}}) = 1 + \frac{1}{\sigma_{\text{tot},3}} \sum_{i=1}^3 \bar{\Sigma}^{(i)}(p_{t,\text{veto}}). \quad (2.4a)$$

In earlier work [5, 13], it had been argued that in order to estimate perturbative uncertainties, one should explore all possible ways of writing the series for $\epsilon(p_{t,\text{veto}})$ that retain the

¹In this respect it differs from the Stewart-Tackmann method [27], which has so far been applied only to fixed-order calculations. An alternative way to estimate the theoretical uncertainties in the resummed case was proposed in [6].

desired perturbative accuracy. For example at N³LO one can introduce scheme (b), as

$$\epsilon^{(b)}(p_{t,\text{veto}}) = 1 + \frac{1}{\sigma_{\text{tot},2}} \sum_{i=1}^3 \bar{\Sigma}^{(i)}(p_{t,\text{veto}}), \quad (2.4b)$$

which is equivalent to scheme (a) up to $\mathcal{O}(\alpha_s^4)$ corrections. Three further schemes are possible at N³LO, where one progressively expands σ_{tot} in the denominator while ensuring the correctness of the full expression at N³LO (see Appendix A). This in effect corresponds to using the degree of convergence for each and every one of the previous orders as an input to determining the possible size of unknown N⁴LO corrections. In the case at hand, however, the early terms of the series show extremely poor convergence, especially at higher energies and when including quark-mass effects. As a result, taking an envelope of all possible schemes leads to uncertainty estimates that grow very large, and contrast with the good convergence observed in practice for the last known order of both the numerator and the denominator. A careful study of this question, summarised in Appendix A, has led us to conclude that it is more appropriate to limit oneself to schemes that give sensitivity to the convergence of just the last order of the perturbative series. This implies that we should take just the two schemes (a) and (b) defined in (2.4).²

Specifically, to estimate our uncertainty for a fixed-order prediction, we will take the envelope of scheme (a) with a 7-point scale variation around a central scale μ_0 ($\mu_{R,F}/\mu_0 = \{\frac{1}{2}, 1, 2\}$ with $\frac{1}{2} \leq \mu_R/\mu_F \leq 2$), together with scheme (b) evaluated at $\mu_{R,F} = \mu_0$. The justification for not having scale variations in scheme (b) is that to include them might effectively correspond to double counting, i.e. summing two sources of uncertainty that may at some level have shared origins.

In the results that follow (unless otherwise specified) we will consider 13 TeV proton–proton collisions, with $R = 0.4$ anti- k_t jets [28] as implemented in FASTJET v. 3.1.2 [29], and use NNPDF2.3 parton distribution functions (PDFs) at NNLO [30], accessed through LHAPDF6 [31], with a strong coupling at the Z -boson mass of $\alpha_s(M_Z) = 0.118$. We choose $\mu_0 = m_H/2$ as the default renormalisation and factorisation scale. No rapidity cuts are applied to the jets.

A comparison of NNLO and N³LO results with this prescription, in the effective theory with a large top mass and no bottom mass, is shown in Fig. 1, for both the jet-veto efficiency (left) and the jet-veto cross section (right). One observes a very considerable decrease in the uncertainties in going from NNLO to N³LO with only a modest change in the central values, associated with a small increase in the total cross section from the N³LO corrections [8] and a slight decrease in the low- p_t efficiency associated with an increase in the 1-jet cross section at NNLO [9–11].

²When the prescription of Refs. [5, 13] was originally introduced, only NNLO results were available. Their last order displayed still rather poor convergence, which justified a more conservative approach.

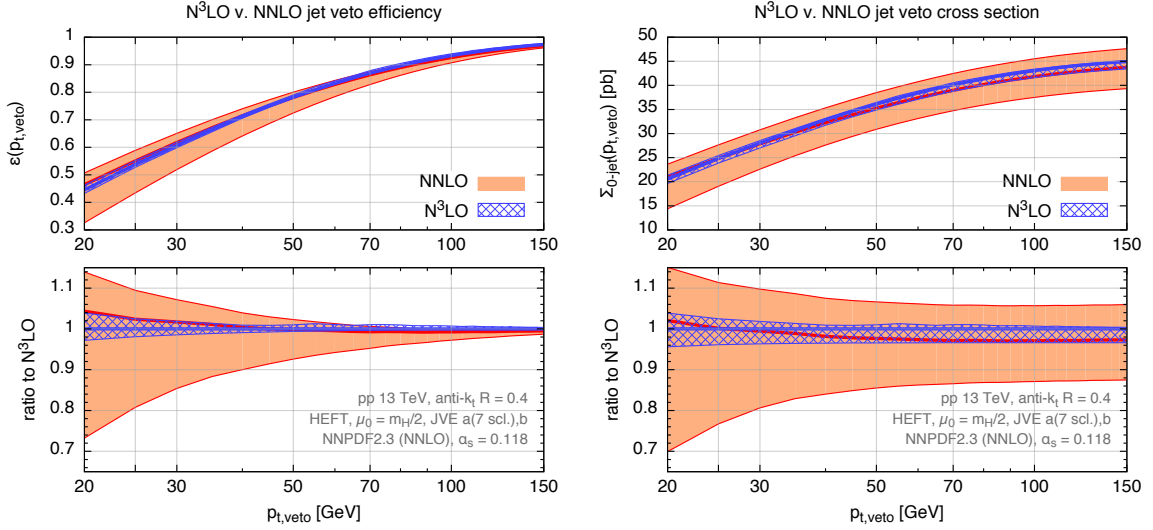


Figure 1. Comparison of NNLO and N³LO results for the jet-veto efficiency (left) and the jet-veto cross section (right), using the updated jet-veto efficiency prescription described in section 2.1. The notation “JVE a(7 scl.),b” indicates the use of the jet efficiency methods with an uncertainty coming from the envelope of 7-point renormalisation and factorisation scale variation in scheme (a) and additionally scheme (b) with central scales.

2.2 Resummation

Next let us recall the structure of the NNLL resummed jet-veto cross section [5],

$$\Sigma_{\text{NNLL}}(p_{t,\text{veto}}) = \left(\mathcal{L}^{(0)}(L) + \mathcal{L}^{(1)}(L) \right) \times \left(1 + \mathcal{F}^{\text{clust}}(R) + \mathcal{F}^{\text{correl}}(R) \right) \times e^{Lg_1(\alpha_s L) + g_2(\alpha_s L) + \frac{\alpha_s}{\pi} g_3(\alpha_s L)}, \quad (2.5)$$

where we have split the factors involving the parton luminosities into two terms $\mathcal{L}^{(0)}(L)$ and $\mathcal{L}^{(1)}(L)$, which start at order α_s^2 and α_s^3 respectively:

$$\begin{aligned} \mathcal{L}^{(0)}(L) &= \sum_{i,j} \int dx_1 dx_2 |M_{B,ij}|^2 \delta(x_1 x_2 s - M^2) f_i(x_1, e^{-L} \mu_F) f_j(x_2, e^{-L} \mu_F), \\ \mathcal{L}^{(1)}(L) &= \frac{\alpha_s}{2\pi} \sum_{i,j} \int dx_1 dx_2 |M_{B,ij}|^2 \delta(x_1 x_2 s - M^2) \left[f_i(x_1, e^{-L} \mu_F) f_j(x_2, e^{-L} \mu_F) \mathcal{H}^{(1)} + \right. \\ &\quad \left. \frac{1}{1 - 2\alpha_s \beta_0 L} \sum_k \left(\int_{x_1}^1 \frac{dz}{z} C_{ik}^{(1)}(z) f_k\left(\frac{x_1}{z}, e^{-L} \mu_F\right) f_j(x_2, e^{-L} \mu_F) + \{(x_1, i) \leftrightarrow (x_2, j)\} \right) \right]. \end{aligned} \quad (2.7)$$

Here $|M_{B,ij}^2|$ is the squared Born matrix element for the partonic scattering channel $ij \rightarrow H$, $L \equiv \ln Q/p_{t,\text{veto}}$ is the logarithm we resum, where typically we choose the resummation scale Q of the order of $m_H/2$. $\mathcal{H}^{(1)}$ is a hard NLO correction, $C_{ik}^{(1)}(z)$ is a NLO coefficient function and $f_i(x, \mu_F)$ is the parton distribution function for flavour i at factorisation scale μ_F . The strong coupling α_s is always understood to be evaluated at a hard scale

$\mu_R \sim m_H/2$, $\beta_0 = (11C_A - 2n_f)/(12\pi)$, and the factorisation scale μ_F is also to be chosen of the order of $m_H/2$. The $g_i(\alpha_s L)$ functions encode the bulk of the LL, NLL and NNLL resummation (for $i = 1, 2, 3$ respectively). The g_2 and g_3 functions, as well as the $\mathcal{H}^{(1)}$ and $C^{(1)}$ coefficients all depend on the choice of Q . The quantities $\mathcal{F}^{\text{clust}}$ and $\mathcal{F}^{\text{correl}}$ [13] account for the NNLL dependence of the result on the jet definition and are further discussed below in section 2.4. Explicit expressions for the above terms are to be found in the supplementary material of Ref. [5], and a number of the elements are closely related to those derived for p_t resummation [32, 33].

2.3 Matching

To put together the fixed-order and resummed results, we use matching schemes that extend those presented in Ref. [5] to one order higher. We refer the reader to that publication for a detailed explanation of the matching procedure. The matching schemes essentially correspond to the two schemes for the fixed-order efficiency given in Eqs. (2.4).

To understand our prescriptions for matching, it is first instructive to rewrite the fixed-order schemes for jet-veto efficiencies as ratios of two cross sections:

$$\epsilon^{(x)}(p_{t,\text{veto}}) \equiv \frac{\Sigma^{(x)}(p_{t,\text{veto}})}{\Sigma^{(x)}(\infty)}, \quad (2.8)$$

where $\Sigma^{(x)}$ admits a different perturbative expansion for each scheme (x) . Specifically, each of the two fixed-order schemes of Eq. (2.4) can be obtained by combining Eq. (2.8) with one of the following prescriptions for Σ :

$$\Sigma^{(a)}(p_{t,\text{veto}}) = \sigma^{(0)} + \Sigma^{(1)} + \Sigma^{(2)} + \Sigma^{(3)}, \quad (2.9a)$$

$$\Sigma^{(b)}(p_{t,\text{veto}}) = \sigma^{(0)} + \Sigma^{(1)} + \Sigma^{(2)} + \bar{\Sigma}^{(3)}. \quad (2.9b)$$

Scheme (a) is the exact expansion for Σ and it trivially gives $\epsilon^{(a)}(p_{t,\text{veto}})$. For scheme (b), observe that it is simply obtained by multiplying $\epsilon^{(b)}$ by $\sigma_{\text{tot},2}$.³

A further standard element that we need is a modification of the resummation so that its effect switches off for $p_{t,\text{veto}} \gtrsim m_H$. We do this by replacing $L \rightarrow \tilde{L}$, defined as

$$\tilde{L} = \frac{1}{p} \ln \left(\left(\frac{Q}{p_{t,\text{veto}}} \right)^p + 1 \right). \quad (2.10)$$

The choice of p is somewhat arbitrary and as in earlier work [13] we take a fairly large value, $p = 5$, to reduce the residual contribution from resummation at high p_t .

³ One could instead arrange for each of the $\Sigma^{(x)}$ to have the property that it tends to $\sigma_{\text{tot},3}$ for $p_{t,\text{veto}} \rightarrow \infty$, however this would complicate the expressions without bringing any actual change in the final results for the jet veto efficiency and cross section.

For the matched cross-sections we obtain the following results:

$$\begin{aligned}
\Sigma_{\text{matched}}^{(a)}(p_{t,\text{veto}}) &= \frac{\Sigma_{\text{NNLL}}(p_{t,\text{veto}})}{\sigma^{(0)}(1 + \delta\mathcal{L}(\tilde{L}))} \left[\sigma^{(0)} \left(1 + \delta\mathcal{L}(\tilde{L}) \right) + \Sigma^{(1)}(p_{t,\text{veto}}) - \Sigma_{\text{NNLL}}^{(1)}(p_{t,\text{veto}}) \right. \\
&\quad + \Sigma^{(2)}(p_{t,\text{veto}}) - \Sigma_{\text{NNLL}}^{(2)}(p_{t,\text{veto}}) + \Sigma^{(3)}(p_{t,\text{veto}}) - \Sigma_{\text{NNLL}}^{(3)}(p_{t,\text{veto}}) \\
&\quad + \left(\delta\mathcal{L}^{(1)}(\tilde{L}) - \frac{\Sigma_{\text{NNLL}}^{(1)}(p_{t,\text{veto}})}{\sigma^{(0)}} + \delta\mathcal{L}^{(2)}(\tilde{L}) - \frac{\Sigma_{\text{NNLL}}^{(2)}(p_{t,\text{veto}})}{\sigma^{(0)}} \right) \\
&\quad \times \left(\Sigma^{(1)}(p_{t,\text{veto}}) - \Sigma_{\text{NNLL}}^{(1)}(p_{t,\text{veto}}) \right) + \left(\delta\mathcal{L}^{(1)}(\tilde{L}) - \frac{\Sigma_{\text{NNLL}}^{(1)}(p_{t,\text{veto}})}{\sigma^{(0)}} \right) \\
&\quad \times \left(\Sigma^{(2)}(p_{t,\text{veto}}) - \Sigma_{\text{NNLL}}^{(2)}(p_{t,\text{veto}}) \right) - \frac{\Sigma_{\text{NNLL}}^{(1)}(p_{t,\text{veto}})}{\sigma^{(0)}} \\
&\quad \times \left. \left(\delta\mathcal{L}^{(1)}(\tilde{L}) - \frac{\Sigma_{\text{NNLL}}^{(1)}(p_{t,\text{veto}})}{\sigma^{(0)}} \right) \left(\Sigma^{(1)}(p_{t,\text{veto}}) - \Sigma_{\text{NNLL}}^{(1)}(p_{t,\text{veto}}) \right) \right], \quad (2.11a)
\end{aligned}$$

$$\Sigma_{\text{matched}}^{(b)}(p_{t,\text{veto}}) = \Sigma_{\text{matched}}^{(a)}(p_{t,\text{veto}}) - \sigma^{(3)} \frac{\Sigma_{\text{NNLL}}(p_{t,\text{veto}})}{\sigma^{(0)}(1 + \delta\mathcal{L}(\tilde{L}))}. \quad (2.11b)$$

In the above expressions, $\Sigma_{\text{NNLL}}^{(n)}(p_{t,\text{veto}})$ denotes the $\mathcal{O}(\alpha_s^n)$ contribution to the NNLL resummed result. The resummed cross section and its expansion are defined in terms of the modified logarithms \tilde{L} as defined in Eq. (2.10). We have also introduced $\delta\mathcal{L} = \mathcal{L}^{(1)}/\mathcal{L}^{(0)}$. This quantity admits a perturbative expansion in powers of α_s , starting at order α_s . We denote this expansion as $\delta\mathcal{L} = \delta\mathcal{L}^{(1)} + \delta\mathcal{L}^{(2)} + \dots$. Note that $\delta\mathcal{L}^{(1)}$ does not actually depend on \tilde{L} . Note also that, as for the fixed-order schemes, the normalisation at $p_{t,\text{veto}} \rightarrow \infty$ is different for each matching scheme, in particular $\Sigma_{\text{matched}}^{(x)}(\infty) = \sigma_{\text{tot},i}$ with $i = 3, 2$ for $x = a, b$. Using Eq. (2.8), one always recovers the correct normalisation $\epsilon(p_{t,\text{veto}}) \rightarrow 1$ for $p_{t,\text{veto}} \rightarrow \infty$.

Since the matching schemes above are multiplicative, for small $p_{t,\text{veto}}$, any finite remainder in the square brackets is multiplied by a Sudakov form factor, ensuring that the cross section and efficiency vanish in the limit $p_{t,\text{veto}} \rightarrow 0$, since $\Sigma_{\text{NNLL}}(p_{t,\text{veto}})$ vanishes in this limit.⁴

For matched results, in addition to varying μ_R and μ_F for scheme (a) and keeping a central choice for scheme (b) (as done in the fixed-order calculations), we also vary Q in scheme (a) around its default choice of $Q_0 = m_H/2$. However, in this work we change our convention for the range of Q variation relative to earlier studies by some of us [5, 13], which had $\frac{1}{2} \leq Q/Q_0 \leq 2$. We instead choose the range of $\frac{2}{3} \leq Q/Q_0 \leq \frac{3}{2}$ that had been originally proposed when Q variation was first introduced [34, 35]. The motivation for returning to this earlier, narrower range comes from the observation of the uncertainties at NNLO+NNLL: with the wider range, the NNLO+NNLL uncertainties come out as unduly large relative the actual changes observed when including N³LO corrections. Moreover, the old variation range gives rise to overly large uncertainties in the tail of the leading jet's

⁴Note that this behaviour of Σ_{NNLL} can be altered when including the small- R resummation. This only happens for rather small R values, and it is therefore not present for phenomenologically relevant values of the jet radius.

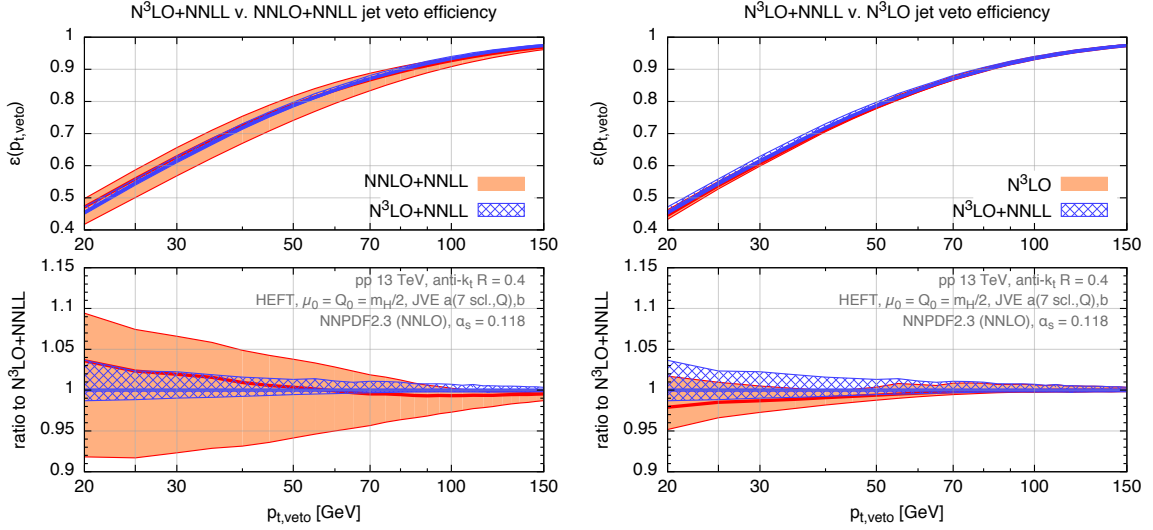


Figure 2. Comparison of matched $N^3\text{LO}+\text{NNLO}$ results for the jet veto efficiency to $\text{NNLO}+\text{NNLL}$ results (left) and to pure $N^3\text{LO}$ predictions (right).

transverse momentum differential spectrum. For a more detailed discussion of this we refer the reader to Appendix A.

Fig. 2 shows the impact of matching the NNLL resummed results with the $N^3\text{LO}$ result, compared to $\text{NNLO}+\text{NNLL}$ results (left) and to pure $N^3\text{LO}$ results (right). In the left-hand plot, one sees a clear reduction in uncertainties in going from $\text{NNLO}+\text{NNLL}$ to $N^3\text{LO}+\text{NNLL}$, as expected given the impact of the $N^3\text{LO}$ results shown in Fig. 1. While the $\text{NNLO}+\text{NNLL}$ results had a substantially smaller uncertainty band than pure NNLO, once one includes one additional order in α_s , resummation brings essentially no further reduction, as is visible in the right-hand plot. It does, however, induce a small shift in the central value (and uncertainty band), whose magnitude is slightly smaller than the uncertainty itself.

2.4 Jet-radius dependence and small- R effects

Two terms in Eq. (2.5) are connected with the choice of jet definition and in particular depend on the jet radius R . $\mathcal{F}^{\text{clust}}(R)$ accounts for clustering of independent soft emissions and for commonly used values of R is given by [5, 13]

$$\mathcal{F}^{\text{clust}}(R) = \frac{4\alpha_s^2(p_{t,\text{veto}})C_A^2 L}{\pi^2} \left(-\frac{\pi^2 R^2}{12} + \frac{R^4}{16} \right). \quad (2.12)$$

$\mathcal{F}^{\text{correl}}(R)$ [13] comes from the correlated part of the matrix element for the emission of two soft partons. For our purposes it is useful to further split it into two parts,

$$\mathcal{F}^{\text{correl}}(R) = \frac{4\alpha_s^2(p_{t,\text{veto}})C_A L}{\pi^2} \left(f_1 \ln \frac{1}{R} + f_{\text{reg}}(R) \right), \quad (2.13)$$

where the coefficient of the logarithm of R is

$$f_1 = \frac{-131 + 12\pi^2 + 132 \ln 2}{72} C_A + \frac{23 - 24 \ln 2}{72} n_f, \quad (2.14)$$

while the finite (regular) remainder is

$$f_{\text{reg}}(R) \simeq 0.6106 C_A - 0.0155 n_f + \mathcal{O}(R^2). \quad (2.15)$$

This was originally derived including terms up to R^6 in Ref. [13] with a numerically-determined constant term, while an analytic form for the constant term and an expansion up to order R^{10} were given in Ref. [7].

Ref. [36] advocated resummation of the terms enhanced by powers of $\ln 1/R$. Ref. [12] showed that LL small- R terms could be incorporated into the jet-veto cross section by replacing $\mathcal{F}^{\text{correl}}(R)$ with

$$\begin{aligned} \mathcal{F}_{\text{LL}_R}^{\text{correl}}(R) = \exp \left[-\frac{4\alpha_s(p_{\text{t,veto}})C_A}{\pi} L \mathcal{Z}(t(R_0, R, p_{\text{t,veto}})) \right] - 1 \\ + \frac{4\alpha_s^2(p_{\text{t,veto}})C_A}{\pi^2} L \left(f_1 \ln \frac{1}{R_0} + f_{\text{reg}}(R) \right), \end{aligned} \quad (2.16)$$

where $\mathcal{Z}(t)$ (denoted $\langle \ln z \rangle_g^{\text{hardest}}(t)$ in Ref. [12]) is the LL_R resummed result for the first logarithmic moment of the momentum fraction carried by the hardest small- R jet resulting from the fragmentation of a gluon. A detailed, partially parametrised, expression for $\mathcal{Z}(t)$ is given in Eq. (C.1), with tabulated coefficients for $n_f = 4, 5$ in table 7 (the second order coefficient was also calculated in Ref. [37]). The quantity $t(R_0, R, p_t)$ is an integral of the coupling over scales related to the allowed emission angles, defined specifically as

$$t(R_0, R, p_{\text{t,veto}}) = \int_{R^2}^{R_0^2} \frac{d\theta^2}{\theta^2} \frac{\alpha_s(p_{\text{t,veto}}\theta)}{2\pi}. \quad (2.17)$$

The nominally free parameter R_0 can be understood as a resummation scale for the LL_R resummation, or, more physically, the largest allowed emission angle. By default we will take $R_0 = 1$ and vary it in the range $0.5 \leq R_0 \leq 2$.

In practice, in Eq. (2.16) we will make the replacements

$$\alpha_s(p_{\text{t,veto}}) = \frac{\alpha_s}{1 - 2\lambda}, \quad (2.18a)$$

$$t(R_0, R, p_{\text{t,veto}}) = \frac{1}{2\pi\beta_0} \ln \frac{1 - 2\lambda}{1 - 2\lambda - \alpha_s\beta_0 \ln \frac{R_0^2}{R^2}}, \quad (2.18b)$$

where $\alpha_s \equiv \alpha_s(\mu_R)$, $\lambda \equiv \alpha_s \tilde{L} \beta_0$. One sees explicitly from Eq. (2.18b) that logarithms of $p_{\text{t,veto}}$ (in λ) and R are being treated on the same footing, i.e. one is including all terms $(\alpha_s \ln p_{\text{t,veto}})^m (\alpha_s \ln R)^n$ for any m and n . The expression includes just the logarithms needed to obtain joint NNLL+ LL_R resummation, without terms that are subleading in this hierarchy (except for those explicitly included as part of a NNLL resummation).⁵

⁵This “minimal” prescription is standard in resummations, however in the limit of sufficiently small R and small $p_{\text{t,veto}}$ we have observed certain artefacts that, as far as we understand, can only be cured by including

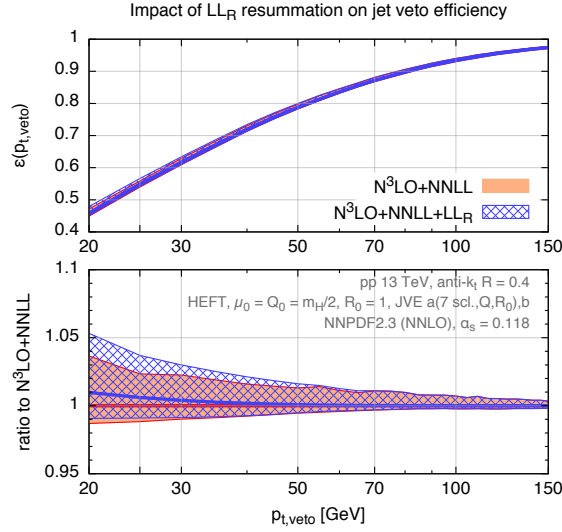


Figure 3. Impact of small- R resummation on the jet-veto efficiency, comparing $N^3\text{LO}+\text{NNLL}+\text{LL}_R$ to $N^3\text{LO}+\text{NNLL}$ results.

The impact of the small- R resummation is shown in Fig. 3, where one sees that it increases the central value of the efficiency by about 1% at $p_{t,\text{veto}} = 20$ GeV, with a slight increase also in the size of the uncertainty band. While it makes sense to include the LL_R resummation with a view to providing the most complete prediction possible, for current phenomenological choices of R it does not bring a large effect.⁶

2.5 Quark-mass corrections

So far we have considered Higgs production in the heavy-top approximation. In this section we study the corrections due to finite top and bottom masses in the loop. Following the procedure of Ref. [23], the effect of heavy-quark masses at NNLL amounts to simply replacing both the Born squared matrix element $|M_{B,ij}|^2$ and the corresponding one-loop virtual correction $\mathcal{H}^{(1)}$ with the ones accounting for the correct quark-masses dependence (cf. section 4.1 of ref. [23]).

We match the NNLL prediction so defined to the $N^3\text{LO}$ fixed-order cross section where we use the exact mass dependence up to NLO, while keeping the heavy-top approximation for both NNLO and $N^3\text{LO}$ corrections. We use this as our default prescription for the results presented below. Moreover, we allow for different resummation scales for top and bottom-induced effects. Therefore, we associate to bottom-induced effects (mainly top-bottom

subleading terms. Furthermore, inspecting the formulae, one immediately sees that the combination of small- R and small- $p_{t,\text{veto}}$ resummation may cause difficulties, since the smallest physical scale in the problem is now $Rp_{t,\text{veto}}$, which for sufficiently small R can approach non-perturbative values even when $p_{t,\text{veto}} \gg \Lambda_{QCD}$. For commonly-used values of the jet radius R and $p_{t,\text{veto}}$ the resummed cross section does not feature this issue, which is irrelevant for the phenomenology shown here. Hence we leave the further study of this question to future work. We thank especially Mrinal Dasgupta for collaboration on this and related aspects.

⁶Ref. [37], using a second order calculation of \mathcal{Z} , had also found small- R effects that were small.

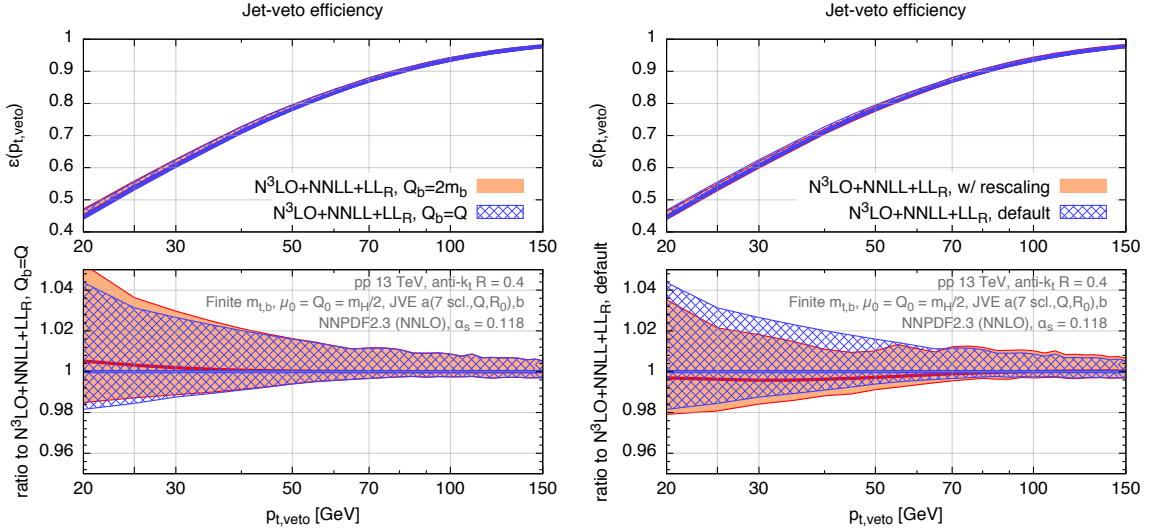


Figure 4. Left: the plot shows the impact of a different resummation scale for the bottom-induced contributions. Our default choice $Q_b = Q$ (in blue/hatched), and it is compared to the result with $Q_b = 2m_b$ (in red/solid). See the text for description. Right: in the plot we compare two different ways of implementing finite quark-mass effects, as discussed in the text.

interference) an additional resummation scale Q_b . The matched cross section, including quark-mass effects then reads

$$\Sigma_{\text{matched}}(p_{t,\text{veto}}) = \Sigma_{\text{matched}}^t(p_{t,\text{veto}}, Q) + \Sigma_{\text{matched}}^{t,b}(p_{t,\text{veto}}, Q_b) - \Sigma_{\text{matched}}^t(p_{t,\text{veto}}, Q_b). \quad (2.19)$$

We set Q to $Q_0 = m_H/2$, and vary it as described in section 2.3 ($\frac{2}{3} \leq Q/Q_0 \leq \frac{3}{2}$) to estimate the associated uncertainty. As far as Q_b is concerned, one could either set $Q_b = Q$ in the jet-veto efficiency (as done in ref. [23]) or set it to small scales of the order of m_b , as advocated in Ref. [22]. As shown in [23], if the resummation is matched to (at least) NNLO, the impact of changing Q_b is very moderate. We show this feature in the left plot of Figure 4 where we compare the jet-veto efficiency obtained with a central $Q_b = 2m_b$ to the one obtained with $Q_b = Q$. In order to be more conservative in our test, we vary Q_b by a factor of two in either direction in the prediction obtained with $Q_b = 2m_b$, while varying it in the nominal range $\frac{2}{3} \leq Q/Q_0 = Q_b/Q_0 \leq \frac{3}{2}$ in the latter case. To this order, the difference between the two prescriptions is minimal. We therefore decide to set $Q_b = Q$ as our central resummation scales and vary them in a correlated way by a factor 3/2 up and down. With this choice the first and third term in the r.h.s. of Eq. (2.19) cancel exactly.

In the context of top-mass corrections only, we note that one could alternatively rescale the NNLO and N³LO corrections by the ratio of the Born cross section with exact top-mass dependence to the corresponding heavy-top result. This rescaling is well justified in the limit of emissions with a transverse momentum much smaller than the top mass. In this region of the spectrum, the corrections to the heavy-top approximation amount to a constant shift up to moderately large $p_{t,\text{veto}}$. This is indeed the region that contributes the most to the total cross section, even more so when a jet veto is applied. However, it is well known that

this is not the case for bottom-quark effects since the region where emissions are softer than the bottom mass is strongly Sudakov-suppressed. This is reflected in the non-trivial shape distortion of the spectrum at normal $p_{t,\text{veto}}$ values [22–24]. Hence, in the small $p_{t,\text{veto}}$ region the above rescaling does not provide a reliable assessment of finite-mass effects.

While it is beyond the scope of this article to give a precise assessment of higher-order mass effects, one can get a rough estimate of their possible impact by comparing our default prescription to the one where one rescales both NNLO and N³LO corrections as discussed above to include finite top-mass effects. We show this in the right-hand plot of Figure 4. We observe very moderate effects of the rescaling down to $p_{t,\text{veto}} = 20$ GeV. This statement is clearly not conclusive, and a more careful study is necessary. Eventually, the issues related to quark-mass effects can only be fixed once a NNLO calculation of mass-effects will be available.

3 N³LO+NNLL+LL_R cross section and 0-jet efficiency at 13 TeV

In this section we report our best predictions for the jet-veto efficiency and cross section at the LHC. The various ingredients that we use were discussed in the previous section, but for ease of reference we summarise them here:

- The total N³LO cross section for Higgs production in gluon fusion [8], obtained in the heavy-top limit.⁷
- The inclusive one-jet cross section at NNLO taken from the code of Ref. [11], in the heavy-top limit. In this computation the $q\bar{q}$ channel is included only up to NLO, and missing NNLO effects are estimated to be well below scale variation uncertainties [10].
- Exact top- and bottom-mass effects up to NLO in the jet-veto efficiency and cross section [14]. Beyond NLO, we use the heavy-top result, as explained in section 2.5.
- Large logarithms $\ln(Q/p_{t,\text{veto}})$ resummed to NNLL accuracy following the procedure of [5], with the treatment of quark-mass effects as described in ref. [23].
- Logarithms of the jet radius resummed to LL accuracy, following the approach of ref. [12].

We consider 13 TeV LHC collisions with a Higgs-boson mass of $m_H = 125$ GeV, compatible with the current experimental measurement [38]. For the top and bottom pole quark masses, we use $m_t = 172.5$ GeV and $m_b = 4.75$ GeV. Jets are defined using the anti- k_t algorithm [28], as implemented in **FastJet** v3.1.2 [29], with radius parameter $R = 0.4$, and perform the momentum recombination in the standard E scheme (i.e. summing the four-momenta of the pseudo-particles). We use NNPDF 2.3 parton distribution functions at NNLO with $\alpha_s(m_Z) = 0.118$ (NNPDF23_nnlo_as_0118) [30].⁸ In our

⁷The Wilson coefficient is expanded out consistently both in the computation of the total and the inclusive one jet cross section.

⁸Note that we use a five-flavour evolution for the running coupling as implemented in **Hoppet** [39], while NNPDF23_nnlo_as_0118 [30] uses a six-flavour scheme. This leads to small differences above the top threshold, which are however numerically irrelevant for our study.

LHC 13 TeV [pb]	$\sigma_{\text{tot},2}$	$\sigma_{\text{tot},3}$	$\sigma_{1j \geq 25\text{GeV}}^{\text{NLO}}$	$\sigma_{1j \geq 25\text{GeV}}^{\text{NNLO}}$	$\sigma_{1j \geq 30\text{GeV}}^{\text{NLO}}$	$\sigma_{1j \geq 30\text{GeV}}^{\text{NNLO}}$
EFT	$45.1^{+4.0}_{-4.6}$	$46.2^{+0.0}_{-1.6}$	$20.3^{+3.6}_{-3.4}$	$21.3^{+0.3}_{-1.3}$	$17.3^{+3.0}_{-2.9}$	$18.1^{+0.2}_{-1.1}$
t -only	$47.1^{+4.3}_{-4.8}$	$48.1^{+0.1}_{-1.9}$	$20.7^{+3.8}_{-3.5}$	$21.8^{+0.4}_{-1.4}$	$17.6^{+3.2}_{-3.0}$	$18.4^{+0.2}_{-1.2}$
t, b	$44.9^{+4.2}_{-4.7}$	$45.9^{+0.0}_{-1.7}$	$20.6^{+3.7}_{-3.5}$	$21.6^{+0.4}_{-1.4}$	$17.6^{+3.2}_{-3.0}$	$18.4^{+0.2}_{-1.2}$

Table 1. Total cross section at NNLO ($\sigma_{\text{tot},2}$) and at N³LO ($\sigma_{\text{tot},3}$), and the one-jet cross-section σ_{1j} at NLO and NNLO for central scales $\mu_0 = m_H/2$, with and without mass effects, as explained in the text. Uncertainties are obtained with a 7-point renormalisation and factorisation scale variation. Numbers determined from the computations of Refs. [8, 9, 11].

central prediction for the jet-veto efficiency we set renormalisation and factorisation scales to $\mu_R = \mu_F = m_H/2$. The resummation scales are set to $Q = Q_b = m_H/2$,⁹ and we use matching scheme (a) (2.11a) as default. In this analysis, we do not include electro-weak corrections [40–42].

To determine the perturbative uncertainties for the jet-veto efficiency we follow the procedure described in section 2.3 and which we summarise here. We vary μ_R, μ_F by a factor of 2 in either direction, requiring $1/2 \leq \mu_R/\mu_F \leq 2$. Maintaining central $\mu_{R,F}$ values, we also vary $Q = Q_b$ in the range $\frac{2}{3} \leq Q/Q_0 = Q_b/Q_0 \leq \frac{3}{2}$. As far as the small- R effects are concerned, we choose the default value for initial radius for the evolution to be $R_0 = 1.0$,¹⁰ and vary it conservatively by a factor of two in either direction. Finally, keeping all scales at their respective central values, we replace the default matching scheme (a) (2.11a) with scheme (b) (2.11b). The final uncertainty band is obtained as the envelope of all the above variations. We do not consider here the uncertainties associated with the parton distributions (which mostly affect the cross section, but not the jet veto efficiency), the value of the strong coupling or the impact of finite quark masses on terms beyond NLO (which was discussed in section 2.5).

We report the numerical values for our input total and one-jet cross section in Table 1, with and without mass effects up to $\mathcal{O}(\alpha_s^3)$, with uncertainties obtained through scale variation and using always NNLO PDFs and α_s .

Figure 5 (left) shows the comparison between our best prediction for the jet-veto efficiency (N³LO+NNLL+LL_R) and the previous NNLO+NNLL accurate prediction, both including mass effects. We see that the impact of the N³LO correction on the central value is of the order of 2% at relevant jet-veto scales. The uncertainty band is significantly reduced when the N³LO corrections are included, going from about 10% at NNLO down to a few percent at N³LO. Figure 5 (right) shows the comparison between the N³LO+NNLL +LL_R prediction and the pure N³LO result. We observe a shift of the central value of the order of 2% for $p_{t,\text{veto}} > 25$ GeV when the resummation is turned on. In that same $p_{t,\text{veto}}$ region, the uncertainty associated with the N³LO prediction is at the 2% level, comparable with

⁹ Q_b applies when including top-bottom interference and bottom contributions, which we do by default here. As shown in section 2.5, switching to the alternative choice $Q_b = 2m_b$ makes less than 1% difference.

¹⁰Note that it acts as a resummation scale for the resummation of logarithms of the jet radius. The initial radius for the small- R evolution differs from the jet radius used in the definition of jets, which is $R = 0.4$.

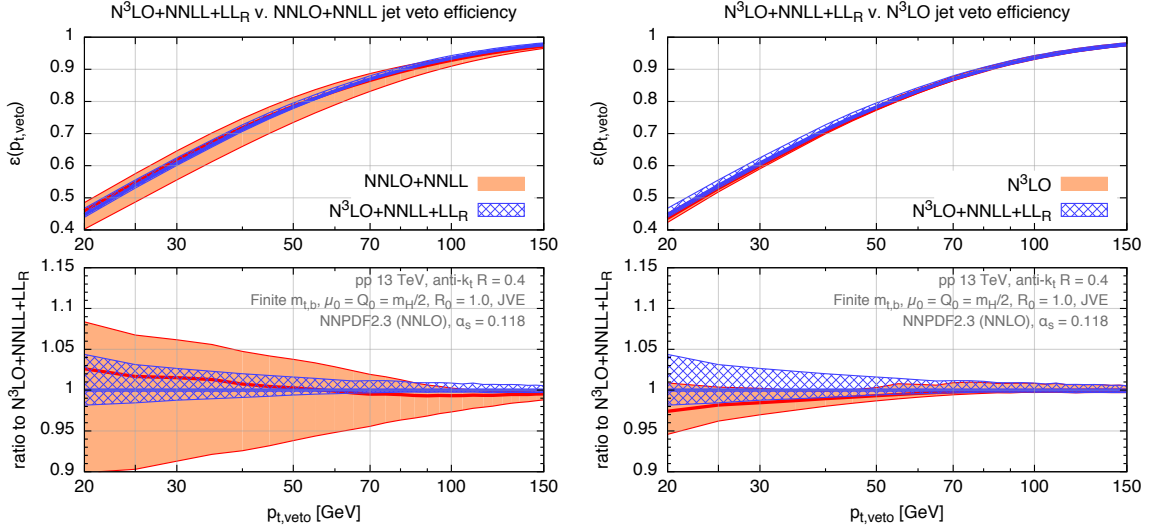


Figure 5. $N^3\text{LO}+\text{NNLL}+\text{LL}_R$ best prediction for the jet-veto efficiency (blue/hatched) compared to $\text{NNLO}+\text{NNLL}$ (left) and fixed-order at $N^3\text{LO}$ (right).

that of the $N^3\text{LO}+\text{NNLL}+\text{LL}_R$ prediction. The fact that resummation effects are of the same order as the uncertainties of the fixed order calculation suggests that the latter might be accidentally small. This situation is peculiar to our central renormalisation and factorisation scale choice, $\mu_R = \mu_F = m_H/2$, and does not occur at, for instance, $\mu_R = \mu_F = m_H$ (see Appendix B for details).

The zero-jet cross section is obtained as $\Sigma_{0\text{-jet}}(p_{t,\text{veto}}) = \sigma_{\text{tot}} \epsilon(p_{t,\text{veto}})$, and the inclusive one-jet cross section is obtained as $\Sigma_{\geq 1\text{-jet}}(p_{t,\text{min}}) = \sigma_{\text{tot}} (1 - \epsilon(p_{t,\text{min}}))$. The associated uncertainties are obtained by combining in quadrature the uncertainty on the efficiency obtained as explained above and that on the total cross section, for which we use plain scales variations. The corresponding results are shown in fig. 6. For this scale choice, we observe that the effect of including higher-order corrections in the zero-jet cross section is quite moderate at relevant $p_{t,\text{veto}}$ scales. This is because the small K factor in the total cross section compensates for the suppression in the jet-veto efficiency. The corresponding theoretical uncertainty is reduced by more than a factor of two.

The predictions for jet-veto efficiency and the zero-jet cross section are summarised in Table 2, for two experimentally relevant $p_{t,\text{veto}}$ choices. Results are reported both at fixed-order, and including the various resummation effects.

Figure 7 shows the inclusive one-jet cross section $\Sigma_{\geq 1\text{-jet}}$, for which the state-of-the-art fixed-order prediction is NNLO [9–11]. The left-hand plot shows the comparison between the best prediction at $\text{NNLO}+\text{NNLL}+\text{LL}_R$, and the fixed-order at NNLO . Both uncertainty bands are obtained with the JVE method outlined in Sec. 2.3. We observe that the effect of the resummation on the central value at moderately small values of $p_{t,\text{veto}}$ is at the percent level. Moreover, the inclusion of the resummation leads to a slight increase of the theory uncertainty in the small transverse momentum region.

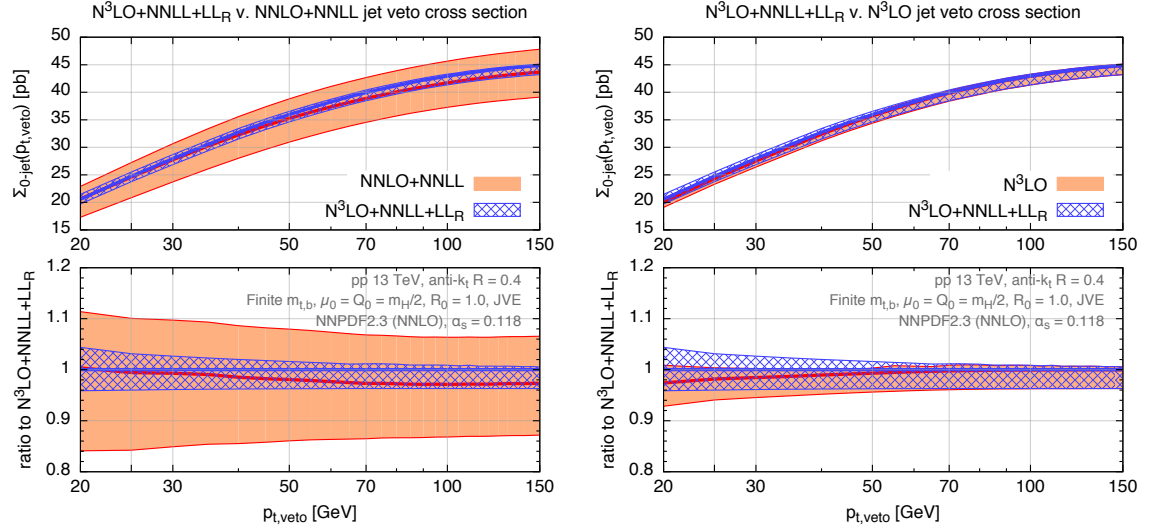


Figure 6. $N^3\text{LO}+\text{NNLL}+\text{LL}_R$ best prediction for the jet-veto cross section (blue/hatched) compared to NNLO+NNLL (left) and fixed-order at $N^3\text{LO}$ (right).

LHC 13 TeV	$\epsilon^{N^3\text{LO}+\text{NNLL}+\text{LL}_R}$	$\Sigma_{0\text{-jet}}^{N^3\text{LO}+\text{NNLL}+\text{LL}_R}$ [pb]	$\Sigma_{0\text{-jet}}^{N^3\text{LO}}$	$\Sigma_{0\text{-jet}}^{\text{NNLO}+\text{NNLL}}$
$p_{t,\text{veto}} = 25 \text{ GeV}$	$0.539^{+0.017}_{-0.008}$	$24.7^{+0.8}_{-1.0}$	$24.3^{+0.5}_{-1.0}$	$24.6^{+2.6}_{-3.8}$
$p_{t,\text{veto}} = 30 \text{ GeV}$	$0.608^{+0.016}_{-0.007}$	$27.9^{+0.7}_{-1.1}$	$27.5^{+0.5}_{-1.1}$	$27.7^{+2.9}_{-4.0}$

Table 2. Predictions for the jet-veto efficiency and cross section at $N^3\text{LO}+\text{NNLL}+\text{LL}_R$, compared to the $N^3\text{LO}$ and NNLO+NNLL cross sections. The uncertainty in the fixed-order prediction is obtained using the JVE method. All numbers include the effect of top and bottom quark masses, treated as described in the text, and are for a central scale $\mu_0 = m_H/2$.

The right-hand plot of Fig. 7 shows our best prediction with uncertainty obtained with the JVE method, compared to the case of just scale (i.e. μ_R , μ_F , Q) variations. We observe a comparable uncertainty both at small and at large transverse momentum, which indicates that the JVE method is not overly conservative in the tail of the distribution. We have observed that the same features persist for the corresponding differential distribution. Table 3 contains the predictions for the inclusive one-jet cross section for two characteristic $p_{t,\text{min}}$ choices.

4 Conclusions

In this article we have presented new state-of-the-art, $N^3\text{LO}+\text{NNLL}+\text{LL}_R$, predictions for the jet-veto efficiency and the zero-jet cross section in gluon-fusion induced Higgs production, as well as NNLO+NNLL+ LL_R results for the inclusive one-jet cross section. The results, shown for 13 TeV LHC collisions, incorporate recent advances in the fixed-order calculation of the total cross section [8], the fixed-order calculation of the one-jet cross section [9–11] and the resummation of small- R effects [12]. They also include the earlier NNLL

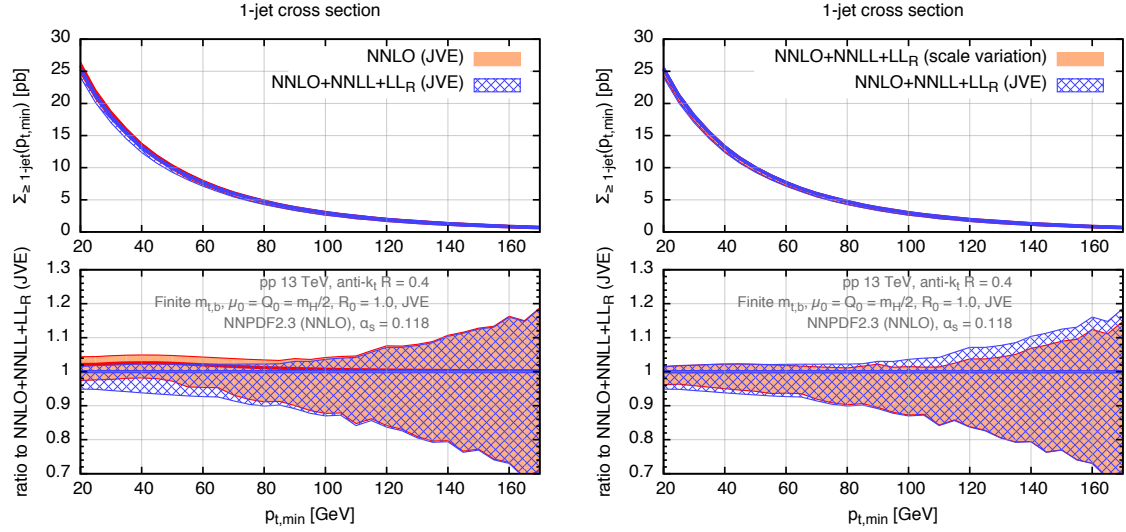


Figure 7. Matched NNLO+NNLL+LL_R prediction for the inclusive one-jet cross section (blue/hatched) compared to fixed-order at NNLO (left) and to the matched result with direct scale variation for the uncertainty (right), as explained in the text.

LHC 13 TeV	$\Sigma_{\geq 1\text{-jet}}^{\text{NNLO+NNLL+LL}_R}$ [pb]	$\Sigma_{\geq 1\text{-jet}}^{\text{NNLO}}$ [pb]
$p_{t,\min} = 25 \text{ GeV}$	$21.2^{+0.4}_{-1.1}$	$21.6^{+0.5}_{-1.0}$
$p_{t,\min} = 30 \text{ GeV}$	$18.0^{+0.3}_{-1.0}$	$18.4^{+0.4}_{-0.8}$

Table 3. Predictions for the inclusive one-jet cross section at NNLO+NNLL+LL_R and NNLO. The uncertainty in the fixed-order prediction is obtained using the JVE method. All numbers include the effect of top and bottom quark masses, treated as described in the text, and are for a central scale $\mu_0 = m_H/2$.

jet p_t resummation [5] including finite quark mass effects [23]. Uncertainties have been determined using the jet-veto efficiency method, which has been updated here to take into account the good perturbative convergence observed with the new fixed-order calculations.

Results for the jet-veto efficiency and zero-jet cross section for central scale choices of $\mu_0 = m_H/2$ and $\mu_0 = m_H$ are reported in tables 2 and 5, respectively. With our central scale choice, $\mu_0 = m_H/2$, we find that the inclusion of the new calculations decreases the jet-veto efficiency by 2% with respect to the NNLO+NNLL prediction, and it has a substantially smaller uncertainty, reduced from more than 10% to less than 5%.

In the zero-jet cross section, the reduction in the jet-veto efficiency is compensated by a similar increase in the total cross section due to the N³LO correction, resulting in a sub-percent effect. In comparison to the N³LO result, the matched N³LO+NNLL+LL_R jet-veto efficiency and zero-jet cross section are about 2% larger, and have comparable ($\sim 3 - 4\%$) theoretical errors. The picture is different for a central scale $\mu_0 = m_H$, as discussed in appendix B. In this case the jet-veto efficiency at N³LO+NNLL+LL_R decreases by more than 5% with respect to the NNLO+NNLL result, while it is in perfect agreement

with the pure $N^3\text{LO}$ prediction. Perturbative uncertainties are considerably (moderately) reduced with respect to the NNLO+NNLL ($N^3\text{LO}$) prediction. For the inclusive one-jet cross section, we find a similar impact of the resummation in the small $p_{t,\text{veto}}$ region, and agreement with the fixed-order scale variation at large transverse momentum values.

We stress that other corrections are of the same order as the theoretical uncertainties obtained here. These involve electro-weak effects, exact quark-mass treatment beyond the orders currently known, and non-perturbative effects. Furthermore, we stress that the results quoted here do not account for PDF and strong coupling uncertainties, which also are at the few-percent level.

Code for performing the resummation and matching with fixed order predictions is publicly available in version 3 of the `JetVHeto` program [43].

Acknowledgements

FC would like to thank Kirill Melnikov and Markus Schulze for collaboration and exchanges concerning the Higgs plus one jet computation. GPS and FAD would like to thank Mrinal Dasgupta, Matteo Cacciari and Gregory Soyez for collaboration in the early stages of the small- R resummation part of this work. We wish to thank Babis Anastasiou, Claude Duhr and Bernhard Mistlberger for interesting discussions regarding the total cross section, and Kirill Melnikov for comments on the manuscript. GZ is supported by the HICCUP ERC Consolidator grant. PM is supported by the Swiss National Science Foundation (SNF) under grant PBZHP2-147297. The work of AB is supported by Science and Technology Facility Council (STFC) under grant number ST/L000504/1. FAD is supported by the ILP LABEX (ANR-10-LABX-63) financed by French state funds managed by the ANR within the Investissements d’Avenir programme under reference ANR-11-IDEX-0004-02. GPS is supported in part by ERC Advanced Grant Higgs@LHC. The work of FD is supported by the Swiss National Science Foundation (SNF) under contract 200021-143781 and by the European Commission through the ERC grant “IterQCD”. AB and PM wish to thank CERN for hospitality, and FC, PM, GS and GZ would like to express a special thanks to the Mainz Institute for Theoretical Physics (MITP) for its hospitality and support while part of this work was carried out.

A Revisited JVE uncertainty prescription

In this paper we argued that the JVE method of ref. [5, 13] used to estimate uncertainties should be modified. In this appendix we wish to motivate why we revisited the JVE prescription. We will argue that, while the original JVE method was appropriate when it was proposed (i.e. when only the NNLO correction to the 0-jet cross section in Higgs production was known), now that the $N^3\text{LO}$ correction is available it would give rise to excessively conservative uncertainties.

It is useful to first recall the original JVE method. In refs. [5, 13], to determine uncertainties in the NNLO+NNLL prediction, μ_R and μ_F were varied by a factor of 2 in either direction, requiring $1/2 \leq \mu_R/\mu_F \leq 2$. Maintaining central $\mu_{R,F}$ values, Q was also

varied by a factor of 2 and changed the matching scheme, from the scheme (a) to schemes (b) and (c) as defined in [5]. The final uncertainty band was the envelope of these variations (cf. [13]). Our new prescription differs from the old one in two important points:

- only schemes (a) and (b) are used to probe the sensitivity to the matching scheme;
- the range for the resummation scale variation is $2/3 \leq Q/Q_0 \leq 3/2$, as suggested originally in ref. [34].

In the rest of this appendix we comment on both of these aspects.

The reason for having different schemes is that the efficiency is a ratio of the jet-vetoed cross section to the total cross section. Even at fixed order there is some freedom as to which perturbative terms one chooses to keep in the denominator, or alternatively expand out. Different matching formulae can then be constructed that reproduce the corresponding fixed-order expansions for the JVE efficiency. At N³LO, in addition to schemes (a) and (b) defined in Eqs. (2.4), one can introduce three further schemes:

$$\epsilon^{(c)}(p_{t,\text{veto}}) = 1 + \frac{1}{\sigma_{\text{tot},1}} \left[\sum_{i=1}^3 \bar{\Sigma}^{(i)}(p_{t,\text{veto}}) - \frac{\sigma^{(2)}}{\sigma_{\text{tot},0}} \bar{\Sigma}^{(1)}(p_{t,\text{veto}}) \right], \quad (\text{A.1a})$$

$$\epsilon^{(c')}(p_{t,\text{veto}}) = 1 + \frac{1}{\sigma_{\text{tot},1}} \left[\sum_{i=1}^3 \bar{\Sigma}^{(i)}(p_{t,\text{veto}}) - \frac{\sigma^{(2)}}{\sigma_{\text{tot},1}} \bar{\Sigma}^{(1)}(p_{t,\text{veto}}) \right], \quad (\text{A.1b})$$

$$\begin{aligned} \epsilon^{(d)}(p_{t,\text{veto}}) = 1 + \frac{1}{\sigma_{\text{tot},0}} \left[\sum_{i=1}^3 \bar{\Sigma}^{(i)}(p_{t,\text{veto}}) - \frac{\sigma^{(1)}}{\sigma_{\text{tot},0}} (\bar{\Sigma}^{(1)}(p_{t,\text{veto}}) + \bar{\Sigma}^{(2)}(p_{t,\text{veto}})) \right. \\ \left. + \frac{\sigma^{(1)}\sigma^{(1)} - \sigma^{(0)}\sigma^{(2)}}{(\sigma_{\text{tot},0})^2} \bar{\Sigma}^{(1)}(p_{t,\text{veto}}) \right]. \quad (\text{A.1c}) \end{aligned}$$

The schemes differ only by terms beyond N³LO.¹¹ At NNLO there are just three schemes, (a), (b) and (c), which respectively have $\sigma_{\text{tot},2}$, $\sigma_{\text{tot},1}$ and $\sigma_{\text{tot},0}$ in the denominator:

$$\epsilon_{\text{NNLO}}^{(a)}(p_{t,\text{veto}}) = 1 + \frac{1}{\sigma_{\text{tot},2}} \sum_{i=1}^2 \bar{\Sigma}^{(i)}(p_{t,\text{veto}}), \quad (\text{A.2a})$$

$$\epsilon_{\text{NNLO}}^{(b)}(p_{t,\text{veto}}) = 1 + \frac{1}{\sigma_{\text{tot},1}} \sum_{i=1}^2 \bar{\Sigma}^{(i)}(p_{t,\text{veto}}), \quad (\text{A.2b})$$

$$\epsilon_{\text{NNLO}}^{(c)}(p_{t,\text{veto}}) = 1 + \frac{1}{\sigma_{\text{tot},0}} \left[\sum_{i=1}^2 \bar{\Sigma}^{(i)}(p_{t,\text{veto}}) - \frac{\sigma^{(1)}}{\sigma_{\text{tot},0}} \bar{\Sigma}^{(1)}(p_{t,\text{veto}}) \right], \quad (\text{A.2c})$$

where, to avoid confusion, here we have explicitly added a “NNLO” label. In what follows, we will drop this label.¹²

To understand why we now restrict the scheme variation to schemes (a) and (b), we first show in Fig. 8 a comparison between the NNLO jet-veto efficiency at 8 TeV and 13 TeV,

¹¹Corresponding formulae for the matching schemes can be found in the documentation of `JetVHeto-v3` [43].

¹²Note that there is a natural correspondence between N³LO and NNLO schemes (a) and (b).

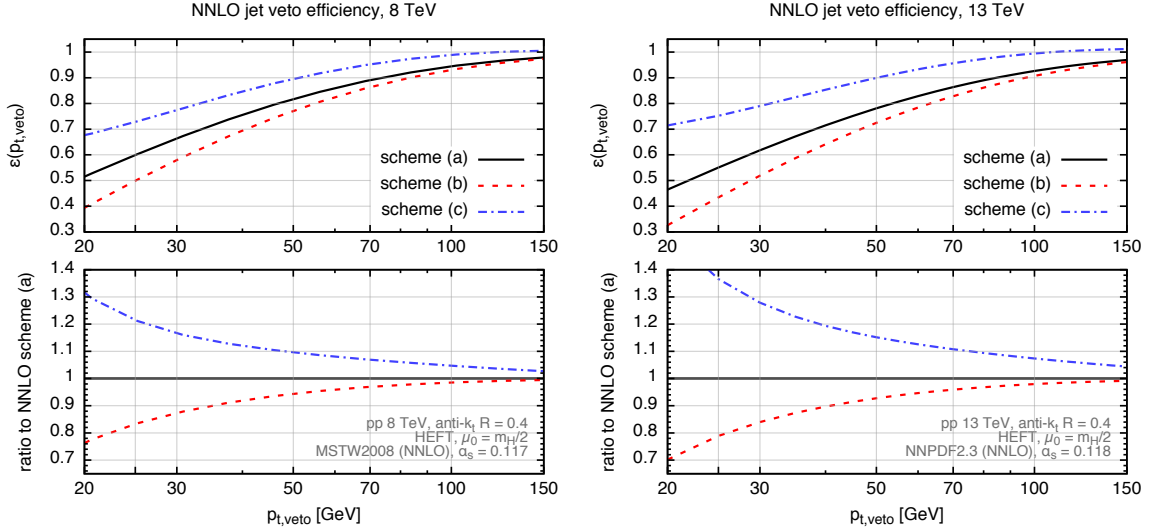


Figure 8. Comparison of the NNLO prediction for the jet-veto efficiency at 8 TeV (left) and 13 TeV (right). The plots show the three efficiency schemes contributing to the uncertainty band in the old formulation of the JVE method.

where we plot the three different possible matching schemes at this order (for the central scale choice). Concentrating first on the absolute values of the efficiency, one sees that in schemes (a) and (b) there is a reduction in going from 8 to 13 TeV. This is consistent with the expectation of an increase in the fraction of events containing a jet when one goes to higher centre-of-mass energy. In contrast, the efficiency increases in scheme (c). This seems unphysical. The combination of the different behaviours of schemes (a) and (c) has the consequence of a very substantial increase in apparent uncertainty. Moreover, at sufficiently high $p_{t,\text{veto}}$ scheme (c) returns an unphysical efficiency $\epsilon^{(c)} > 1$.

The issues with scheme (c) are to some extent understood, since scheme (c) at NNLO is very sensitive to the convergence of the first correction in the perturbative expansion. It is well-known that the first terms for the Higgs cross section converge very poorly. In particular, the ratio of NLO to LO cross section contributions, $\sigma^{(1)}/\sigma^{(0)}$, goes from about 1.23 to 1.30 between 8 and 13 TeV.¹³ The difference between schemes (a) and (b), on the other hand, is only sensitive to the size of the last perturbative order, hence we believe it provides useful, but not overly conservative, information on the uncertainty.

In order to study the impact of the new prescription for the efficiency scheme variation, in Fig. 9 we show the fixed-order efficiency at NNLO and N³LO, concentrating on the 13 TeV case, where the impact of scheme (c) (at NNLO) and (d) (at N³LO) is more pronounced. Fig. 9 shows the various efficiency schemes contributing at a given order according to the old JVE prescription. We see that at N³LO the spread between schemes (a) and (b) is comparable with the change in the efficiency from NNLO to N³LO, while the inclusion of additional schemes (c), (c') and (d) gives rise to a much larger uncertainty. This suggests

¹³The $\sigma^{(1)}/\sigma^{(0)}$ ratio is further enhanced when mass effects are included.

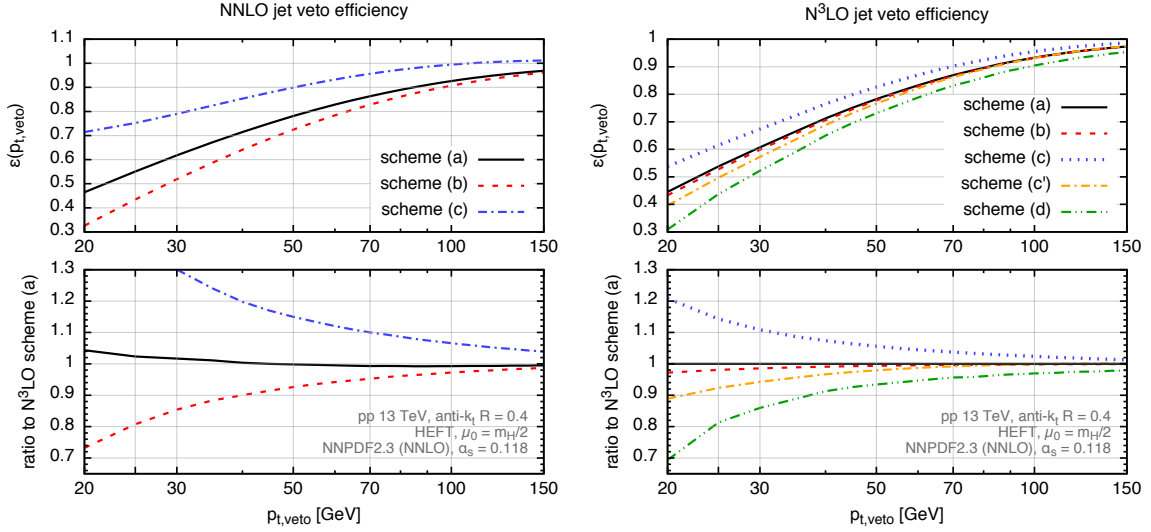


Figure 9. Jet-veto efficiency at 13 TeV. The plots show the various efficiency schemes at NNLO (left) and N³LO (right). The lower panels show the ratio to the N³LO central prediction (scheme (a)).

that the old JVE prescription is overestimating uncertainties at this c.o.m. energy. This is even more true when including finite quark-mass effects (not shown here).

It is however also clear that, since the (b) scheme prediction is obtained by computing the jet-veto efficiency at the central scale only, if the N³LO correction to the total cross section is accidentally very small at that scale, schemes (a) and (b) will return nearly identical values. Therefore, the corresponding scheme uncertainty will be very small. For our central scale $\mu_0 = m_H/2$ the N³LO correction is in fact very small (2.4%) and, accordingly, the corresponding scheme spread in the right-hand plot of Fig. 9 is very small. To investigate whether this is a general feature of the new scheme prescription, one can examine the uncertainty band at a different central scale. We have done this in App. B, where it is shown that in that case the scheme variation contributes significantly to the size of the theoretical uncertainty.

An alternative way to address the issue of accidentally small scheme (b) variation is to introduce a prescription that probes the scheme variation at different scales (where the size of the N³LO corrections may be more sizeable). For instance, one could determine the scheme uncertainty by adding to the usual envelope the spread between schemes (a) and (b) at different scales. We therefore investigate the following (b:a) prescription: to define the uncertainty band, we take the envelope of scheme (a) with its set of 7 scale variations (and Q and R_0 variations) and additionally the 7 scale variations of

$$\epsilon_{\mu_0, \mu_0}^{(a)}(p_{t,\text{veto}}) + \epsilon_{\mu_R, \mu_F}^{(b)}(p_{t,\text{veto}}) - \epsilon_{\mu_R, \mu_F}^{(a)}(p_{t,\text{veto}}), \quad (\text{A.3})$$

where we have included explicit subscript labels for the renormalisation and factorisation scales. By sampling Eq. (A.3) over 7 scale choices, one explores the maximum difference between schemes (a) and (b) (with identical scale choices for the two schemes) and applies

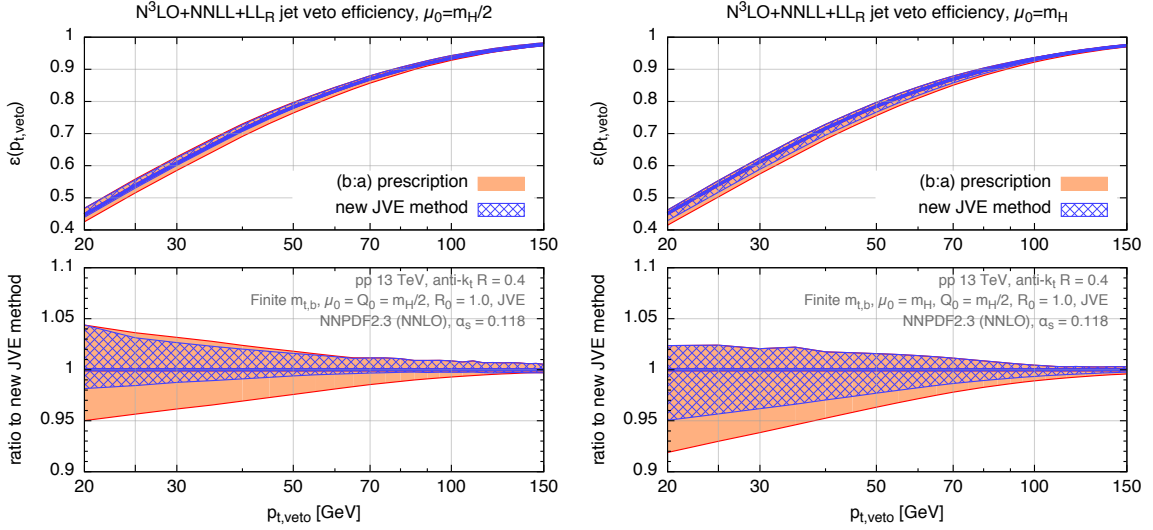


Figure 10. Jet-veto efficiency with uncertainty band obtained with our nominal JVE method and with the $(b:a)$ prescription as described in the text at central scales $\mu_0 = m_H/2$ (left) and $\mu_0 = m_H$ (right).

that difference as an additional uncertainty relative to the result of scheme (a) for its central scale choice $\mu_R = \mu_F = \mu_0$. In this way one avoids the problem that the difference between schemes (b) and (a) may be accidentally small for the central scale choice. This approach also avoids the potential risk of double counting of uncertainties that would come were one simply to take the envelope of schemes (a) and (b) , each with 7 scale variations.

The comparison between the new JVE prescription to the $(b:a)$ procedure is shown in Fig 10. We see that the $(b:a)$ prescription gives rise to only marginally larger uncertainties. Moreover, we have found that the $(b:a)$ prescription gives rise to enlarged uncertainties in the tail of the leading jet p_t distribution. For these reasons, and due the fact that this procedure is more cumbersome and relies on a non-standard method to assess the error, we do not adopt it as our default prescription.

Besides the different efficiency scheme variation, another important difference between our new JVE prescription and the original one [13] is the range of variation for the resummation scale Q . Instead of varying it in the range $\{m_H/4, m_H\}$ as done originally, we now restrict ourselves to the smaller range $\{m_H/3, 3/4 m_H\}$. The main reason for this is that one wants the one-jet cross section at large p_t to be insensitive to the resummation, therefore one should ensure that the resummation is correctly turned off at large $p_{t,\text{veto}}$ values. The scale at which the resummation is turned off is determined by the resummation scale Q . Making the choice $Q = m_H$ has the effect of starting the resummation in a region of relatively high p_t , where the underlying soft and collinear approximations are far from being valid.

In the left-hand plot of Fig. 11 we show the one-jet cross section at NNLO+NNLL+LL_R with uncertainties obtained with the new formulation of the JVE method both with a Q variation range of $\{m_H/4, m_H\}$ (green/hatched band) and $\{m_H/3, 3/4 m_H\}$ (blue/hatched).

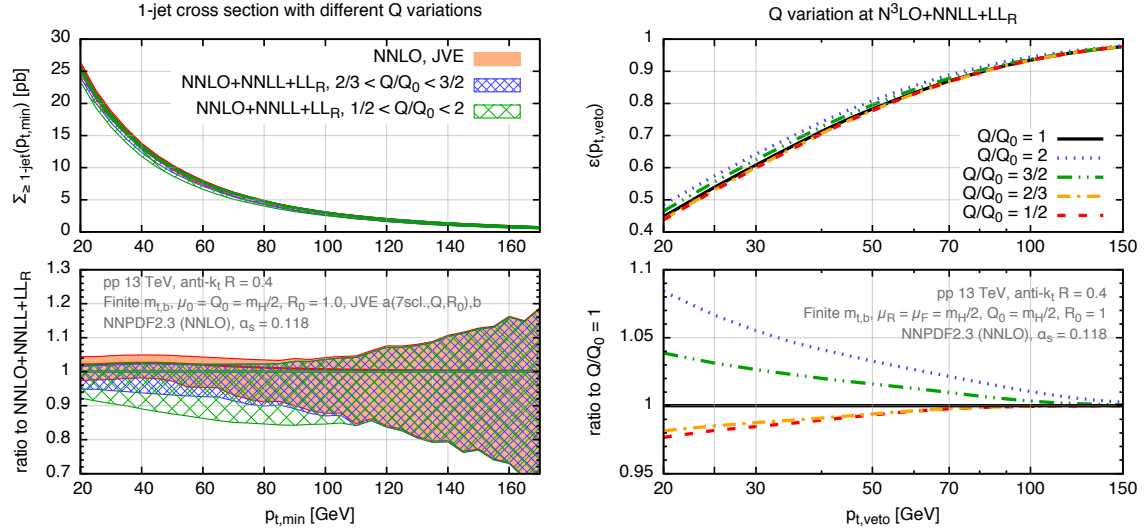


Figure 11. Left: one-jet cross section at NNLO (red/solid band) and NNLO+NNLL+LL_R (blue/hatched band), with uncertainty obtained with the new JVE method as described in the text, compared to the NNLO+NNLL+LL_R with a Q variation in the range $\{m_H/4, m_H\}$ (green/hatched). Right: jet-veto efficiency at N³LO+NNLL+LL_R for different values of the resummation scale Q , as used in the old ($Q/Q_0 = 1/2$, $Q/Q_0 = 2$) and new ($Q/Q_0 = 2/3$, $Q/Q_0 = 3/2$) formulations of the JVE method, where $Q_0 = m_H/2$.

The fixed order result (red/solid) is also shown for comparison. We observe that while the effect of resummation on the central value is very moderate, the band obtained with the old Q variation range is substantially larger all the way up to $p_t \sim 100$ GeV. The right-hand plot of Fig. 11 shows the jet-veto efficiency at N³LO+NNLL+LL_R for the values of the resummation scale Q used in the old ($Q = m_H/4$, $Q = m_H$) and in the new ($Q = m_H/3$, $Q = 3/4 m_H$) prescription for the JVE method. While the curve corresponding to the upper variation changes significantly when reducing Q from m_H to $3/4 m_H$, the curve corresponding to the lower edge is largely unaffected by the change in the variation range. The insensitivity to the choice of the lower end of the range for Q motivates a simple symmetric choice for the resummation scale range.

Finally, it is interesting to see how the original prediction of ref. [5] changes with the new prescription for the JVE uncertainty. Fig. 12 shows the comparison between the old and new JVE methods for the NNLO+NNLL efficiency at 8 TeV. We observe that the new prescription leads to a reduction of the upper part of the uncertainty band. At low values of $p_{t,veto}$ this reduction is mainly driven by the reduction in the Q variation range (cf. Fig. 11), while at large $p_{t,veto}$ scheme (c) gives a significant contribution to the theoretical uncertainty (cf. Fig. 8). To conclude this section, we remark that when the original formulation of the JVE method was proposed, the NNLO corrections showed a somewhat problematic convergence, therefore a more conservative approach to the uncertainty estimate seemed appropriate. Now that the computation of the N³LO correction shows a much better convergence of the perturbative series, extensive study has led us to believe that the new

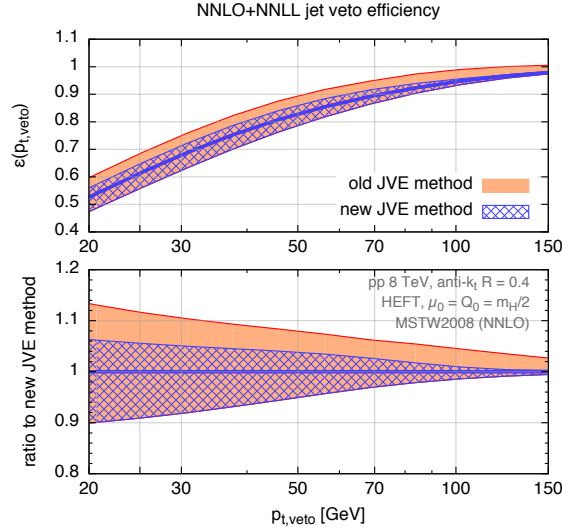


Figure 12. Jet-veto efficiency at NNLO+NNLL at 8 TeV with uncertainty bands obtained with the original formulation of the JVE method [5] (red/solid) compared to the prediction obtained with the new JVE method as defined in the text (blue/hatched).

formulation of the JVE method is more appropriate.

B Choice of the central scale

Results presented in the main text are obtained using $m_H/2$ as a central scale choice. This choice, rather than m_H , is motivated by the better convergence of the perturbative expansion and by the fact that soft emissions and virtual corrections that contribute substantially to the cross-section tend to have scales that are typically lower than m_H . It is similar also to the choice of $H_T/2$ or $p_{t,\text{jet}}$ that is often used in processes with more complex final states. Nevertheless it is interesting to examine how much our central results and the uncertainties change when m_H is adopted as a central scale.

Table 4 shows the input numerical values for the total and one-jet cross section, with and without mass effects, up to $\mathcal{O}(\alpha_s^3)$, with uncertainties obtained through scale variation and using NNLO PDFs and α_s using a central scale m_H . These numbers are to be compared to those at scale $m_H/2$, Table 1.

In Fig. 13 we show a comparison of the $\text{N}^3\text{LO} + \text{NNLL} + \text{LL}_R$ results to NNLO+NNLL results (left) and to N^3LO (right) at central scale m_H . This figure is to be compared to the similar one at central scale $m_H/2$, Fig. 5. It is clear that at scale m_H uncertainties are somehow larger, this is particularly the case for the N^3LO prediction. Accordingly, uncertainty bands overlap slightly better at scale m_H . Still, the change in the central value at $\text{N}^3\text{LO} + \text{NNLL} + \text{LL}_R$ is very small when using m_H rather than $m_H/2$. The corresponding plots for the 0-jet cross section are shown in Fig. 14. Results for the efficiency and 0-jet cross section are reported in Tab. 5.

LHC 13 TeV [pb]	$\sigma_{\text{tot},2}$	$\sigma_{\text{tot},3}$	$\sigma_{1j \geq 25 \text{ GeV}}^{\text{NLO}}$	$\sigma_{1j \geq 25 \text{ GeV}}^{\text{NNLO}}$	$\sigma_{1j \geq 30 \text{ GeV}}^{\text{NLO}}$	$\sigma_{1j \geq 30 \text{ GeV}}^{\text{NNLO}}$
EFT	$41.1^{+4.4}_{-4.3}$	$44.8^{+1.3}_{-2.5}$	$16.9^{+3.5}_{-2.9}$	$20.2^{+1.4}_{-2.0}$	$14.4^{+3.0}_{-2.5}$	$17.1^{+1.2}_{-1.6}$
t -only	$42.9^{+4.7}_{-4.5}$	$46.6^{+1.6}_{-2.7}$	$17.3^{+3.5}_{-3.0}$	$20.6^{+1.4}_{-2.0}$	$14.6^{+3.0}_{-2.5}$	$17.4^{+1.2}_{-1.6}$
t, b	$40.8^{+4.6}_{-4.3}$	$44.5^{+1.5}_{-2.5}$	$17.1^{+3.5}_{-3.0}$	$20.5^{+1.4}_{-2.0}$	$14.6^{+3.0}_{-2.5}$	$17.4^{+1.2}_{-1.6}$

Table 4. Total cross section at NNLO ($\sigma_{\text{tot},2}$) and at N³LO ($\sigma_{\text{tot},3}$), and the one-jet cross-section σ_{1j} at NLO and NNLO for central scale $\mu_0 = m_H$, with and without mass effects as explained in the text. Uncertainties are obtained with a 7-point renormalisation and factorisation scale variation.

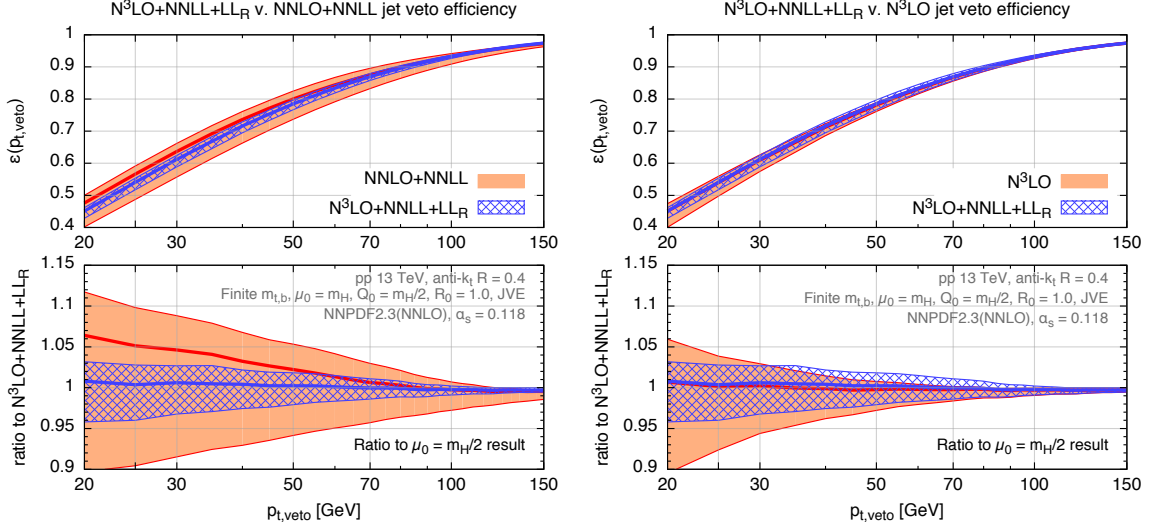


Figure 13. N³LO+NNLL+LL_R best prediction for the jet-veto efficiency (blue/hatched) compared to NNLO+NNLL (left) and fixed-order at N³LO (right) at $\mu_0 = m_H$. The lower panel shows the ratio to the $\mu_0 = m_H/2$ result.

LHC 13 TeV	$\epsilon^{\text{N}^3\text{LO}+\text{NNLL}+\text{LL}_R}$	$\Sigma^{\text{N}^3\text{LO}+\text{NNLL}+\text{LL}_R}_{0\text{-jet}}$ [pb]	$\Sigma^{\text{N}^3\text{LO}}_{0\text{-jet}}$	$\Sigma^{\text{NNLO}+\text{NNLL}}_{0\text{-jet}}$
$p_{t,\text{veto}} = 25 \text{ GeV}$	$0.541^{+0.013}_{-0.023}$	$24.0^{+1.0}_{-1.7}$	$24.0^{+1.2}_{-2.3}$	$23.1^{+2.8}_{-4.0}$
$p_{t,\text{veto}} = 30 \text{ GeV}$	$0.612^{+0.013}_{-0.023}$	$27.2^{+1.1}_{-1.9}$	$27.1^{+1.2}_{-2.2}$	$25.9^{+3.1}_{-4.2}$

Table 5. Predictions for the jet-veto efficiency and cross section at N³LO+NNLL+LL_R, compared to the N³LO and NNLO+NNLL cross sections. The uncertainty in the fixed-order prediction is obtained using the JVE method. All numbers include the effect of top and bottom quark masses, treated as described in the text, and are for a central scale $\mu_0 = m_H$.

To gain insight into the differences between the two scale choices, Fig. 15 shows the breakdown into different sources of uncertainty using $m_H/2$ (left) and m_H (right) as a central scale choice. We notice that for the central scale $m_H/2$ the full uncertainty band is determined by the scale variations (both Q and μ_R, μ_F), while scheme and R_0 variation give rise to a lower uncertainty. For central scale m_H the upper edge of the band is still

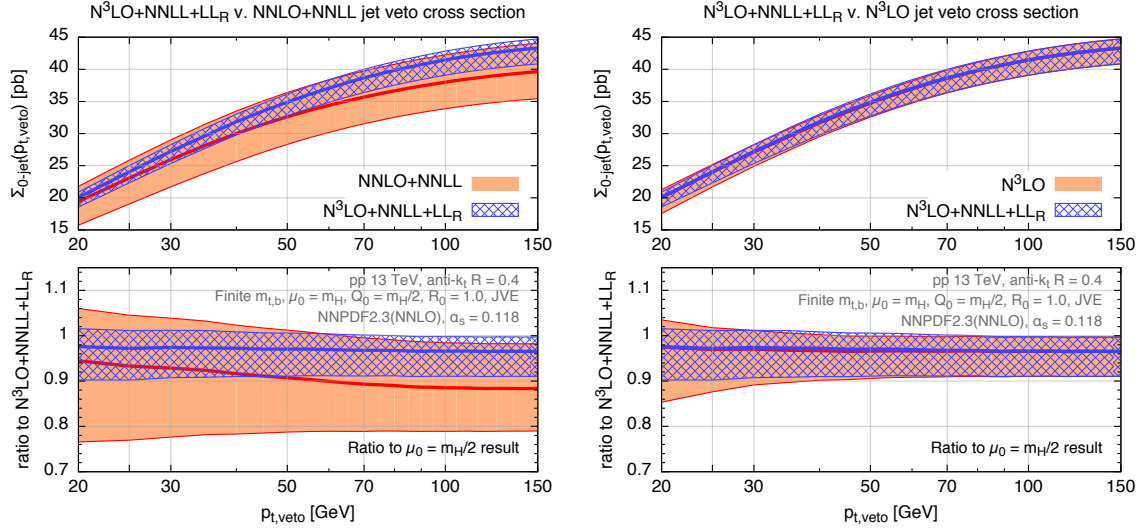


Figure 14. $N^3\text{LO}+\text{NNLL}+\text{LL}_R$ best prediction for the jet-veto cross section (blue/hatched) compared to NNLO+NNLL (left) and fixed-order at $N^3\text{LO}$ (right) at $\mu_0 = m_H$. The lower panel shows the ratio to the $\mu_0 = m_H/2$ result.

LHC 13 TeV	$\Sigma_{\geq 1\text{-jet}}^{\text{NNLO}+\text{NNLL}+\text{LL}_R}$ [pb]	$\Sigma_{\geq 1\text{-jet}}^{\text{NNLO}}$ [pb]
$p_{t,\min} = 25 \text{ GeV}$	$20.4^{+1.2}_{-1.3}$	$20.5^{+2.0}_{-1.5}$
$p_{t,\min} = 30 \text{ GeV}$	$17.2^{+1.2}_{-1.1}$	$17.3^{+1.7}_{-1.2}$

Table 6. Predictions for the inclusive one-jet cross section at NNLO+NNLL+LL_R and NNLO. The uncertainty in the fixed-order prediction is obtained using the JVE method. All numbers include the effect of top and bottom quark masses, treated as described in the text, and are for a central scale $\mu_0 = m_H$.

set by scale variation, while the lower one is determined by the scheme variation, and R_0 variation has still no impact on the final uncertainty band. The difference in the impact of the scheme variation at the two different scales is a consequence two facts: (a) at scale $m_H/2$ the $N^3\text{LO}$ correction is only a 2% correction, while it amounts to 9% at scale m_H ; and (b) in our updated JVE approach, the scheme-variation is now sensitive only to the ambiguity of including (or not) the $N^3\text{LO}$ correction to the total cross section in the efficiency.

Next, in Fig. 16 we show the inclusive one-jet cross section (blue/hatched) compared to fixed-order at NNLO (left) and to the matched result with direct scale variation for the uncertainty as explained in the text (right) at central scale m_H . Corresponding numerical values for the one-jet cross section are reported in Tab. 6. From the right-hand plot of Fig. 16, one notices that the JVE uncertainty band, especially its upper edge, is larger than scale variation even at transverse momenta of the order of m_H . This larger uncertainty for the JVE result appears to be associated with the variation between schemes (a) and (b), which differ by about 10% over a range of $p_{t,\min}$, a consequence of the nearly 10% difference between $\sigma_{\text{tot},2}$ and $\sigma_{\text{tot},3}$ that is visible in table 4. This effect is not present for the results

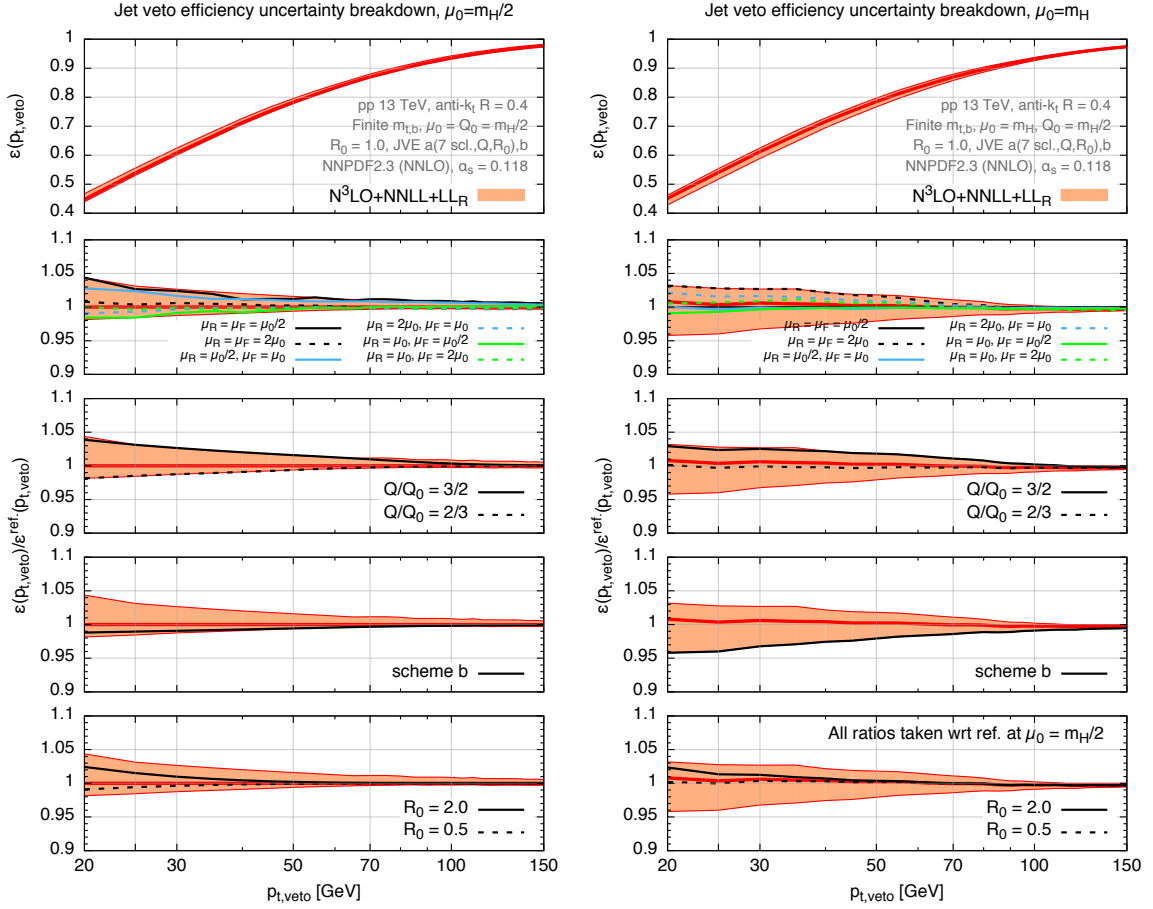


Figure 15. $N^3\text{LO}+\text{NNLL}+\text{LL}_R$ best prediction for the jet-veto efficiency (red band), with a breakdown (lower panels) comparing the overall relative uncertainty envelope to the different contributions from which it is built up. The left and right-hand plots show results respectively for scale choices $\mu_0 = m_H/2$ and m_H . In both plots, ratios are taken with respect to a reference result determined with $\mu_0 = m_H/2$.

with central scale $\mu_0 = m_H/2$, Fig. 7, where the difference between the two schemes is much smaller. However, for large values of $p_{t,\min}$ the uncertainty on the $\mu_0 = m_H/2$ results grows more rapidly, perhaps a consequence of the fact such a scale choice is not appropriate at high p_t .

C Small- R correction factor

In Ref. [12], small- R effects for jet vetoes were resummed through the introduction of a “fragmentation” function $f^{\text{hardest}}(z, t)$ for the distribution of the momentum fraction z carried by the hardest subjet resulting from the fragmentation of a gluon. The quantity

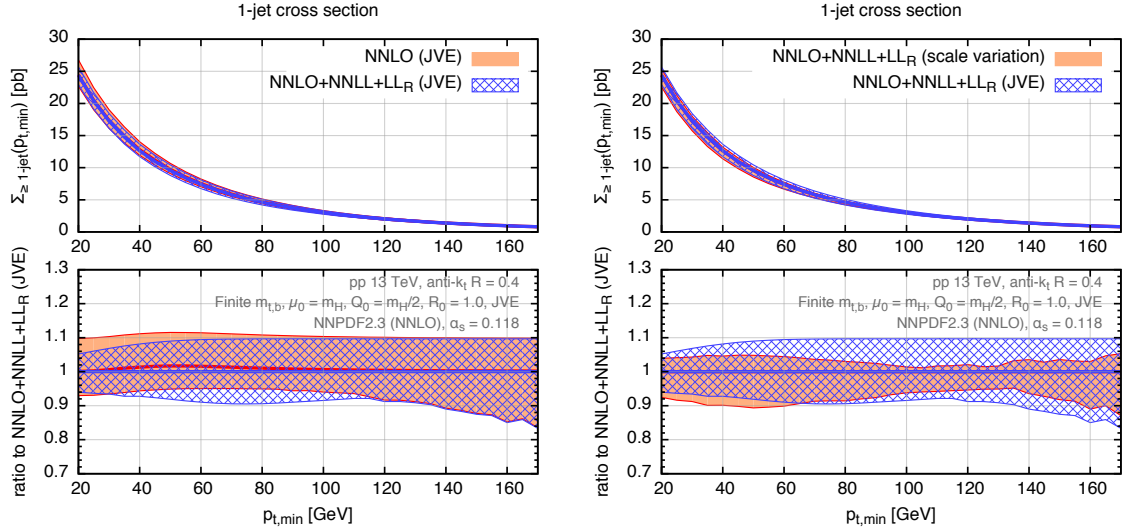


Figure 16. Best prediction for the inclusive one-jet cross section (blue/hatched) compared to fixed-order at NNLO (left) and to the matched result with direct scale variation for the uncertainty as explained in the text (right). The central renormalisation and factorisation scales are set to $\mu_0 = m_H$. The lower panel shows the ratio to the central value at $\mu_0 = m_H$.

$\mathcal{Z}(t)$ used in Eq. (2.16) is the first logarithmic moment of this fragmentation function,

$$\begin{aligned}
\mathcal{Z}(t) &\equiv \int_0^1 dz f^{\text{hardest}}(z, t) \ln z \\
&\simeq t \left[\frac{1}{72} C_A (131 - 12\pi^2 - 132 \ln 2) + \frac{1}{36} n_f T_R (-23 + 24 \ln 2) \right] \\
&+ \frac{t^2}{2!} (0.206672 C_A^2 + 0.771751 C_A n_f T_R \\
&\quad - 0.739641 C_F n_f T_R + 0.117861 n_f^2 T_R^2) \\
&+ \frac{t^3}{3!} (-0.20228(4) C_A^3 - 0.53612(2) C_A^2 n_f T_R - 0.062679(8) C_A C_F n_f T_R \\
&\quad + 0.54199(2) C_F^2 n_f T_R - 0.577215(3) C_A n_f^2 T_R^2 \\
&\quad + 0.431055(4) C_F n_f^2 T_R^2 - 0.0785743(5) n_f^3 T_R^3) \\
&+ \frac{t^4}{4!} c_4^{\text{fit}} + \frac{t^5}{5!} c_5^{\text{fit}} + \frac{t^6}{6!} c_6^{\text{fit}} + \frac{t^7}{7!} c_7^{\text{fit}} + \frac{t^8}{8!} c_8^{\text{fit}}, \tag{C.1}
\end{aligned}$$

where the coefficients up to t^3 are the actual terms of the full Taylor expansion of $\mathcal{Z}(t)$, while those from t^4 to t^8 , given in table 7, are chosen so as to provide a good fit to the full numerical form for $\mathcal{Z}(t)$ as calculated in Ref. [12]. Coefficients are tabulated both for $n_f = 4$ and $n_f = 5$.¹⁴ As such, these higher order coefficients are not the actual values of the coefficients of the Taylor series for $\mathcal{Z}(t)$, since yet higher-order contributions might be partly absorbed in the fit. Eq. (C.1) reproduces the full all-order result at the per mil

¹⁴The results of this paper use the $n_f = 5$ values.

	c_4^{fit}	c_5^{fit}	c_6^{fit}	c_7^{fit}	c_8^{fit}
$n_f = 5$	133.55	-478.55	-1226.87	22549.99	-77020.08
$n_f = 4$	100.69	-352.10	-858.44	15819.97	-53597.50

Table 7. Results of a fit to parametrise the all-order result of the integral in Eq. (C.1). Values are given for $n_f = 4$ and $n_f = 5$. The fitted curve is accurate to 0.1% in the $t \in [0, 1]$ range.

level in the range $0 < t < 1$, which should be more than adequate for phenomenological applications.

For the purposes of matching, it is useful to have the α_s expansion of $\mathcal{F}_{\text{LLR}}^{\text{correl}}(R)$ up to α_s^3 . The $\alpha_s^2 L$ and $\alpha_s^3 L^2$ terms are known from previous work. Once one includes LL_R resummation there is an additional $\alpha_s^3 L \ln^2 R$ term, which receives contributions from both the order t and t^2 terms in Eq. (C.1), because t itself has an all-order expansion in powers of $\alpha_s \ln R$. It is given by

$$\mathcal{F}_{\text{LLR},31}^{\text{correl}}(R) = \left(\frac{\alpha_s}{2\pi}\right)^3 L \cdot 16C_A \ln^2 \frac{R}{R_0} \left[1.803136C_A^2 - 0.589237n_f 2T_R C_A \right. \\ \left. + 0.36982C_F n_f 2T_R - 0.05893n_f^2 4T_R^2 \right]. \quad (\text{C.2})$$

References

- [1] G. Aad *et al.* [ATLAS Collaboration], Phys. Lett. B **716** (2013) 1 [arXiv:1207.7214 [hep-ex]].
- [2] S. Chatrchyan *et al.* [CMS Collaboration], Phys. Lett. B **716** (2013) 30 [arXiv:1207.7235 [hep-ex]].
- [3] G. Aad *et al.* [ATLAS Collaboration], Phys. Rev. D **92** (2015) 1, 012006 [arXiv:1412.2641 [hep-ex]].
- [4] S. Chatrchyan *et al.* [CMS Collaboration], JHEP **1401** (2014) 096 [arXiv:1312.1129 [hep-ex]].
- [5] A. Banfi, P. F. Monni, G. P. Salam and G. Zanderighi, Phys. Rev. Lett. **109** (2012) 202001 [arXiv:1206.4998 [hep-ph]].
- [6] I. W. Stewart, F. J. Tackmann, J. R. Walsh and S. Zuberi, Phys. Rev. D **89** (2014) 5, 054001 [arXiv:1307.1808].
- [7] T. Becher, M. Neubert and L. Rothen, JHEP **1310** (2013) 125 [arXiv:1307.0025 [hep-ph]].
- [8] C. Anastasiou, C. Duhr, F. Dulat, F. Herzog and B. Mistlberger, Phys. Rev. Lett. **114** (2015) 212001 [arXiv:1503.06056 [hep-ph]].
- [9] R. Boughezal, F. Caola, K. Melnikov, F. Petriello and M. Schulze, Phys. Rev. Lett. **115** (2015) 8, 082003 [arXiv:1504.07922 [hep-ph]].
- [10] R. Boughezal, C. Focke, W. Giele, X. Liu and F. Petriello, Phys. Lett. B **748** (2015) 5 [arXiv:1505.03893 [hep-ph]].
- [11] F. Caola, K. Melnikov and M. Schulze, Phys. Rev. D **92** (2015) 7, 074032 [arXiv:1508.02684 [hep-ph]].
- [12] M. Dasgupta, F. Dreyer, G. P. Salam and G. Soyez, JHEP **1504** (2015) 039 [arXiv:1411.5182 [hep-ph]].

- [13] A. Banfi, G. P. Salam and G. Zanderighi, JHEP **1206** (2012) 159 [arXiv:1203.5773 [hep-ph]].
- [14] M. Spira, A. Djouadi, D. Graudenz and P. M. Zerwas, Nucl. Phys. B **453** (1995) 17 [hep-ph/9504378].
- [15] M. Spira, Fortsch. Phys. **46** (1998) 203 [hep-ph/9705337].
- [16] R. Harlander and P. Kant, JHEP **0512** (2005) 015 [hep-ph/0509189].
- [17] C. Anastasiou, S. Beerli, S. Bucherer, A. Daleo and Z. Kunszt, JHEP **0701** (2007) 082 [hep-ph/0611236].
- [18] U. Aglietti, R. Bonciani, G. Degrossi and A. Vicini, JHEP **0701** (2007) 021 [hep-ph/0611266].
- [19] R. Bonciani, G. Degrossi and A. Vicini, JHEP **0711** (2007) 095 [arXiv:0709.4227 [hep-ph]].
- [20] T. Neumann and M. Wiesemann, JHEP **1411** (2014) 150 [arXiv:1408.6836 [hep-ph]].
- [21] H. Mantler and M. Wiesemann, Eur. Phys. J. C **73** (2013) 6, 2467 [arXiv:1210.8263 [hep-ph]].
- [22] M. Grazzini and H. Sargsyan, JHEP **1309** (2013) 129 [arXiv:1306.4581 [hep-ph]].
- [23] A. Banfi, P. F. Monni and G. Zanderighi, JHEP **1401** (2014) 097 [arXiv:1308.4634 [hep-ph]].
- [24] E. Bagnaschi, G. Degrossi, P. Slavich and A. Vicini, JHEP **1202** (2012) 088 [arXiv:1111.2854 [hep-ph]].
- [25] E. Bagnaschi and A. Vicini, arXiv:1505.00735 [hep-ph].
- [26] K. Hamilton, P. Nason and G. Zanderighi, JHEP **1505** (2015) 140 [arXiv:1501.04637 [hep-ph]].
- [27] I. W. Stewart and F. J. Tackmann, Phys. Rev. D **85** (2012) 034011 [arXiv:1107.2117 [hep-ph]].
- [28] M. Cacciari, G. P. Salam and G. Soyez, JHEP **0804**, 063 (2008) [arXiv:0802.1189 [hep-ph]].
- [29] M. Cacciari, G. P. Salam and G. Soyez, Eur. Phys. J. C **72**, 1896 (2012) [arXiv:1111.6097 [hep-ph]].
- [30] R. D. Ball, V. Bertone, S. Carrazza, C. S. Deans, L. Del Debbio, S. Forte, A. Guffanti and N. P. Hartland *et al.*, Nucl. Phys. B **867** (2013) 244 [arXiv:1207.1303 [hep-ph]].
- [31] A. Buckley, J. Ferrando, S. Lloyd, K. Nordström, B. Page, M. Rüfenacht, M. Schönherr and G. Watt, Eur. Phys. J. C **75** (2015) 3, 132 [arXiv:1412.7420 [hep-ph]].
- [32] G. Bozzi, S. Catani, D. de Florian and M. Grazzini, Nucl. Phys. B **737** (2006) 73 [hep-ph/0508068].
- [33] T. Becher and M. Neubert, Eur. Phys. J. C **71** (2011) 1665 [arXiv:1007.4005 [hep-ph]].
- [34] M. Dasgupta and G. P. Salam, JHEP **0208** (2002) 032 [hep-ph/0208073].
- [35] R. W. L. Jones, M. Ford, G. P. Salam, H. Stenzel and D. Wicke, JHEP **0312** (2003) 007 [hep-ph/0312016].
- [36] F. J. Tackmann, J. R. Walsh and S. Zuberi, Phys. Rev. D **86** (2012) 053011 [arXiv:1206.4312 [hep-ph]].
- [37] S. Alioli and J. R. Walsh, JHEP **1403** (2014) 119 [arXiv:1311.5234 [hep-ph]].
- [38] G. Aad *et al.* [ATLAS and CMS Collaborations], arXiv:1503.07589 [hep-ex].

- [39] G. P. Salam and J. Rojo, Comput. Phys. Commun. **180** (2009) 120 [arXiv:0804.3755 [hep-ph]].
- [40] S. Actis, G. Passarino, C. Sturm and S. Uccirati, Phys. Lett. B **670** (2008) 12 [arXiv:0809.1301 [hep-ph]].
- [41] C. Anastasiou, R. Boughezal and F. Petriello, JHEP **0904** (2009) 003 [arXiv:0811.3458 [hep-ph]].
- [42] W. Y. Keung and F. J. Petriello, Phys. Rev. D **80** (2009) 013007 [arXiv:0905.2775 [hep-ph]].
- [43] <https://jetvheto.hepforge.org/>.